Geological Society of America
Special Paper 405
2006

Microfacies and origin of some Archean cherts (Pilbara, Australia)

Beate Orberger†
Departement des Sciences de la Terre, UMR IDES 8148, Interaction et Dynamique des Environnements de Surface, Universite Paris Sud, Bât. 504, 91405 Orsay Cedex, France
Virgile Rouchon
Departement des Sciences de la Terre, UMR IDES 8148, Interaction et Dynamique des Environnements de Surface, Universite Paris Sud, Bât. 504, 91405 Orsay Cedex, France and
Department of Earth and Space Sciences, Graduate School of Science, Osaka University, Toyonaka, Osaka 560-0043, Japan
Frances Westall
Centre de Biophysique Moleculaire, CNRS, Rue Charles Sadron, 45071 Orleans cedex 2, France
Sjoukje T. de Vries
Faculty of Geosciences, Utrecht University, Budapestlaan 4, 3584 CD Utrecht, The Netherlands
Daniele L. Pinti
Departement des Sciences de la Terre et de l'Atmosphère, Universite du Quebec à Montreal et GEOTOP-UQAM-McGill, C.P. 8888, Succ. Centre-Ville, Montreal, QC H3C 3P8, Canada
Christiane Wagner
Laboratoire de Petrologie-PMMP, CNRS-FR32, Universite Paris VI, 4 Place Jussieu, 75251 Paris cedex, France
Richard Wirth
GeoForschungsZentrum Potsdam, Department 4, Telegrafenberg, D-14482 Potsdam, Germany
Ko Hashizume
Department of Earth and Space Sciences, Graduate School of Science, Osaka University, Toyonaka, Osaka 560-0043, Japan

ABSTRACT

Four cherts sampled in the East Pilbara craton (Western Australia) at Marble Bar (Towers Formation), North Pole Dome (Dresser and Apex Basalt Formation), and Kittys Gap (Panorama Formation) were studied for micro- and nanomineralogy and geochemistry to determine their protoliths and to provide new insights on the physico-chemical and biological conditions of their depositional environments. The Marble Bar chert was formed at the interface with a basaltic rock. Hydrothermal fluids leached major and trace elements from the basalt and silicified the protolith of this chert. The elements Fe, Mn, Si, Ca, Mg, REE, Au, Pd, Cr, and Ni precipitated as a microbanded iron formation (BIF) under reducing and alkaline conditions. The chert is composed of magnetite, carbonates, and quartz and forms a stromatolite-like structure. Later oxidizing fluids replaced magnetite and carbonates with Fe-Mn oxyhydroxides. They show vermicular microtextures and filamentous nanotextures. Each filament is composed of euhedral nanoscopic hematite. These oxides contain several thousands of ppm of N and C, and measured C/N ratios are similar to those observed in organic matter preserved in marine sediments, thus suggesting an organic activity.

†E-mail: orberger@geol.u-psud.fr.

Orberger, B., Rouchon, V., Westall, F., de Vries, S.T., Pinti, D.L., Wagner, C., Wirth, R., and Hashizume, K., 2006, Microfacies and origin of some Archean cherts (Pilbara, Australia), *in* Reimold, W.U., and Gibson, R.L., Processes on the Early Earth: Geological Society of America Special Paper 405, p. 133–156, doi: 10.1130/2006.2405(08).

Two black cherts from hydrothermal dykes of the North Pole Dome are interpreted as having had a black shale precursor, based on the REE (rare earth elements) and trace metal characteristics. These rocks were probably entrained into the dykes and hydrothermally overprinted. Although these two cherts had the same history, the physico-chemical conditions differed during their formation. The chert from the chert-barite unit of the Dresser Formation was formed under reducing and alkaline conditions. This is clearly indicated by clusters of nanosulfide spherules replacing precursor minerals; weblike Fe-sulfides intergrown with sphalerite; As-pyrite and vaesite; and the presence of carbonates. The black chert from the Apex Basalt Formation was formed under oxidizing conditions, as indicated by clusters of nanospherules of Fe-oxides and a negative Ce anomaly.

A black and white laminated chert from Kittys Gap was formed in a shallow marine to subaerial environment, by silicification of a rhyodacitic volcaniclastic rock. This process was accompanied by the development of microbial mats on the sediment surfaces and the formation of microbial colonies around precursor K-feldspars, Ti-bearing biotites, amphiboles, and ghost spherulites. The environment was slightly oxidizing, as indicated by the negative Ce anomaly and the presence of Ti-oxides. The presence of K-bearing phyllosilicates rather than K-feldspars indicates that the environment was also slightly acidic. Elevated Cu and Zn contents in the black laminae point to a limited influence from hydrothermal fluids. The silica probably originated mainly from alteration of the minerals of the volcaniclastic rock due to diagenetic alteration by seawater.

Keywords: Archaean sediments, chert, Banded Iron Formations, iron oxyhydroxides, microbial activity.

INTRODUCTION

Archean cherts are at the center of much debate because they are considered to host the first traces of early life, either as physical (e.g., stromatolites, microbial mats, bacteriomorph structures) or chemical signatures (N, C, and S) interpreted as being derived from biological activity (Schidlowski et al., 1983; Byerly et al., 1986; Walsh, 1992; Beaumont and Robert, 1999; Westall et al., 2001, this volume; Pinti et al., 2001b). These siliceous rocks can have different origins depending on their environment of formation. In modern and Paleozoic settings (Grenne and Slack, 2003a, 2003b), silica can precipitate at mid-ocean ridges (MOR) (Halbach et al., 2002), in shallow littoral subaquatic (Tarasov et al., 1999), or in lacustrine environments (Eugster, 1967; Schubel and Simonson, 1990; Umeda, 2003; Renaut et al., 2002). In the latter case, they are known as siliceous sinter deposits and occur in hot springs related to geothermal activity. Fluid temperatures at the surface are generally below 100 °C, but reservoir temperatures vary from 175 to 350 °C (Fournier and Rowe, 1966). Modern hydrothermal environments contain microorganisms (mostly prokaryotes) that can be rapidly mineralized and, thus, have a high preservation potential in the geological record (Cady and Farmer, 1996). Cherts can also form by replacement of preexisting magmatic (volcanic or plutonic) or sedimentary rocks, by silica metasomatism (de Wit et al., 1982; Pirajno and Grey, 2002; Orberger et al., 2005a), or they can be of biogenic-organic origin (such as diatomites, radiolarites; e.g., Beauchamp and Baud, 2002). The latter circumstances are not considered to be relevant in the Archean.

The analysis of biogenicity in Archean cherts needs an integrated, multidisciplinary approach to analyze depositional conditions and subsequent diagenetic or metamorphic transformations, which can modify the primary biogenic and abiogenic signatures (Farmer and Des Marais, 1999; Grotzinger and Knoll, 1995). In this paper, we report the results of analysis of four Archean chert samples from the Pilbara craton: a chert from the Marble Bar, Towers Formation; two cherts from the North Pole Dome, belonging to the Dresser and Apex Basalt Formation, and a chert from the Kittys Gap locality of the Coppin Belt, Panorama Formation (Fig. 1). We used micromineralogy and REE–geochemistry to reconstruct the depositional environments for these rocks and their physico-chemical conditions during silicification.

GEOLOGICAL SETTINGS

The four cherts belong to the Warrawoona Group of the East Pilbara Greenstone Belt, Western Australia (Fig. 1). The Marble Bar chert (sample A458; UTM AMG50, 782100E, 7654600N) belongs to the A-section of the Towers Formation (Kato and Nakamura, 2003; Fig. 1). Following the sampling scheme of Kato and Nakamura (2003), the sample was obtained from a horizon 2251–2308 cm from the bottom of the section. The A-section is the thickest (45 m thick) stratum in this forma-

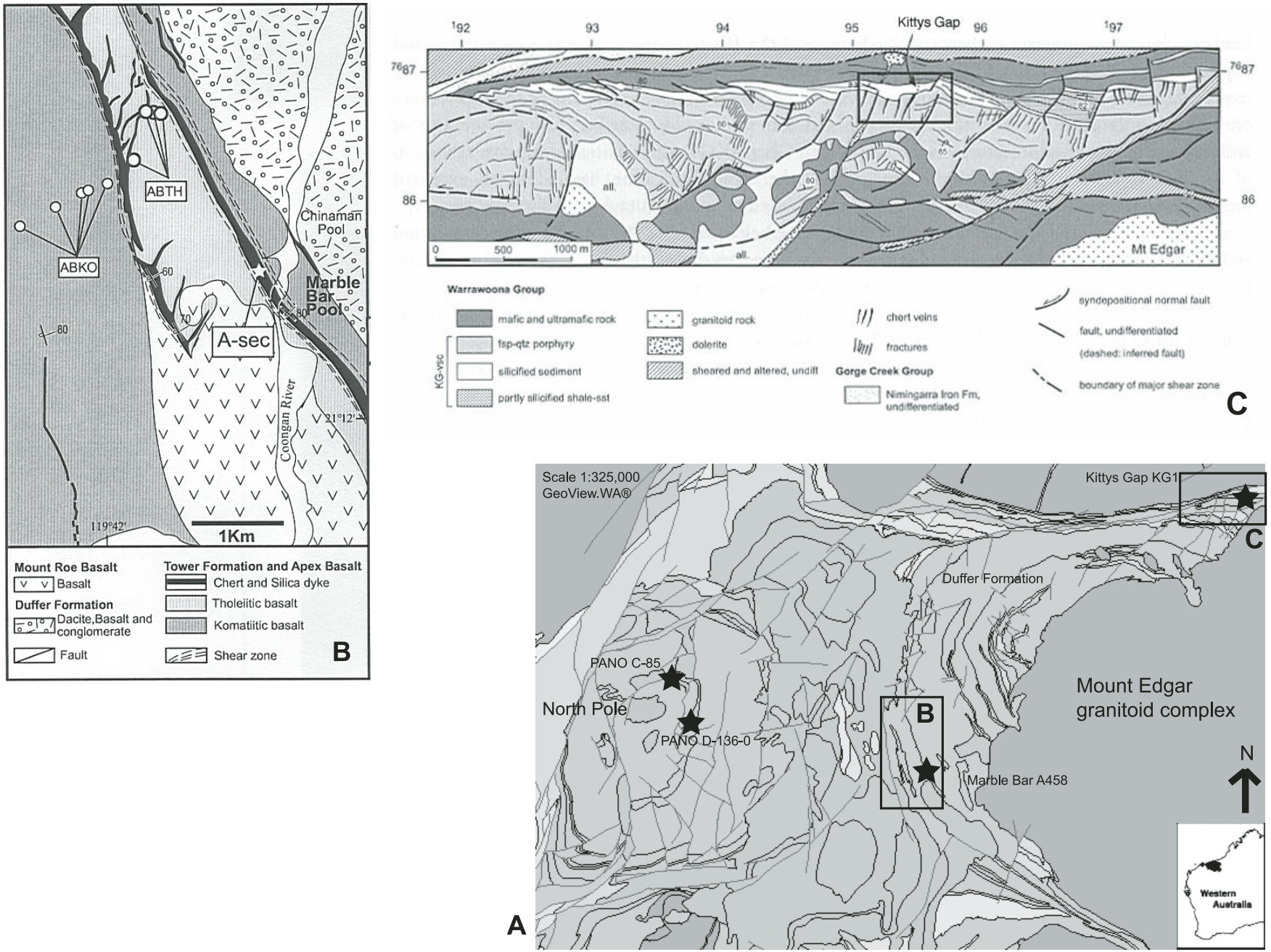

Figure 1. Simplified geological map of a part of Western Australia with the sampling positions of the studied cherts PANO D-136–0 and PANO C-85, A458 and KG-1. Map source (modified): Department of Industry and Resources of Western Australia, http://www.doir.wa.gov.au/aboutus/geoview_launch.asp.

tion. It is composed of highly ferruginous cherts directly overlying Fe-rich, K-poor, tholeiitic basalts having MORB–type (mid-oceanic-ridge basalt) geochemical patterns (Kato and Nakamura, 2003). The estimated depositional age of the Marble Bar Chert Unit is between 3474 and 3433 Ma (Thorpe et al., 1992; van Kranendonk et al., 2001). The interpretation of the depositional environment of the Marble Bar belt is controversial. Suggestions range from a volcanic- or near-arc setting, based on the chemical composition of the tholeiitic and calc-alkaline basalts (Barley, 1993; Kitajima et al., 2001), to an oceanic plateau setting, based on the association of tholeiites and komatiites (Condie, 1997). The cherts from the A-section have been recently interpreted as in situ precipitates from a high-temperature hydrothermal solution emanating from a MOR (Kato and Nakamura, 2003).

Chert sample PANO D-136–0 (UTM AMG50 754300E, 7662100N; previously named PANO D-136 *in* Pinti et al., 2001b) represents the North Pole Dome locality (Van Kranendonk et al., 2001) and belongs to the Talga-Talga Subgroup, Dresser Formation, Chert-Barite Unit (Fig. 1). This unit has an estimated depositional age of 3490 Ma (Thorpe et al., 1992). The Dresser Formation (Towers Formation in the former stratigraphical scheme of the area, Van Kranendonk et al., 2001) is composed of five horizons of stromatolitic chert-barite horizons, interbedded with pillow basalts. The sample studied here is a black chert from one of the numerous silica dykes that were emplaced within and immediately above listric normal growth faults that were active during chert deposition (Y. Isozaki, 1997, personal commun.; Van Kranendonk et al., 2001). These silica dykes have been recently interpreted as hydrothermal veins (Isozaki et al., 1999; Nijman et al., 1998; van Kranendonk et al., 2001; Ueno et al., 2004) and are possibly the remains of white hydrothermal smokers (Nijman et al., 1998). The silica would have been precipitated from hydrothermal fluids during a lacco-caldera formation (Nijman et al., 1998; van Kranendonk et al., 2001).

Chert sample PANO C-85 (UTM AMG50 751900E, 7667100N) is a zoned black and white chert from a vein that has been stratigraphically assigned to the 3465-Ma-old Salgash Subgroup, Apex Basalt Formation, Apex Chert Unit (Y. Ueno, 2004, personal commun.). Pinti et al. (2001a) erroneously related it to the volcaniclastic, felsic rock-rich Panorama Formation. The Apex Basalt Formation is dominated by pillow basalts, which are largely tholeiitic. A number of mainly black and white, well-laminated chert horizons are interbedded with the volcanics. Numerous chert dykes cut across the underlying stratigraphy and terminate at the level of the chert horizons (Lindsay et al., 2003).

The Kittys Gap locality (UTM AMG50 195200E, 7687200N) belongs to the Coppin Gap greenstone belt, north of the Mount Edgard Complex (Figs. 1A and 1C). The Coppin Gap is a weakly metamorphosed stratigraphic sequence of basalt and felsic volcanics and siliceous sedimentary rocks, offset by normal faults (Nijman et al., 1998; Van Kranendonk et al., 2001; de Vries, 2004). The felsic rocks, grading from rhyolitic to dacitic toward the top, belong to the Panorama Formation (de Vries, 2004). The chert from Kittys Gap, sample KG 1, comes from the 3446 Ma Panorama Formation, Kittys Gap Chert lower unit (de Vries, 2004). The outcrop is composed of a small-scale, heteroclitic, ripple-laminated chert.

ANALYTICAL METHODS

Polished thin sections were studied with a reflected and transmitted light optical microscope and by scanning electron microscopy (SEM, Philips XL 30) at the University of Paris Sud, France. Semiquantitative chemical analyses were performed at 20–30 kV using an EDX-PGT Ge-detector installed on the SEM. Some samples were etched for 5 s in 10 times diluted HNO_3 and later observed at 5 kV and analyzed at 10kV with field emission gun scanning electron microscopy (FEG-SEM of the Hitachi S 3400 type at the University of Orléans, France).

Major and trace element whole rock analyses were carried out at the SARM-CRPG (Centre de Recherches Pétrographiques et Géochimiques) of Nancy, France. The samples were fused with $LiBO_2$, dissolved in HNO_3, analyzed by inductive coupled plasma atomic emission spectrometry (ICP-AES: major and minor elements) and inductive coupled plasma mass spectrometry (ICP-MS: trace elements), and calibrated with international standards. Selenium was determined by Atomic Absorption Spectroscopy (AAS). Sulfur and CO_2 were analyzed using infrared absorptiometry. Organic carbon was obtained through calcination at 1400 °C, after destruction of the carbonates. The FeO contents were analyzed by volumetry. For details on the precision and detection limits, see the appendix. Trace elements in the Fe-Mn–oxides, carbonates, sulfides, and hydromuscovites were analyzed by electron microprobe (Cameca SX50®) at the Centre de Microanalyses de Paris (CAMPARIS) Center, Université Pierre et Marie Curie of Paris, France. Counting time for each element was 10 s. Standards were diopside (Mg, ca), orthoclase (K, Al), pyrophanite (Mn, Ti), Cr_2O_3 (Cr), Fe_2O_3 (Fe), ZnS (Zn), NiO (Ni), Co metal (Co), and Cu metal (Cu). Detection limits are at the hundred ppm level. Representative analyses are shown in Tables 1A–1D. Focused-ion beam (FIB) transmission electron microscopy was performed at the GeoForschungsZentrum (GFZ) in Potsdam (Germany). The method applied is described in Wirth (2004).

Results

Marble Bar Chert–Towers Formation (A458)

Mineralogy. Sample A458 is a composite chert consisting of a dark gray part (zone I), a microbanded iron formation a few millimeters thick (micro–BIF, zone II), and a light gray part (zone III, Fig. 2A). Transmitted light microscopy indicates that, prior to silicification, the precursor rock of zone I had a porphyritic or porphyroclastic texture, typical of volcanic or volcaniclastic rocks. Euhedral to subhedral phenocrysts were replaced by microcrystalline quartz. These replacement structures sometimes contain euhedral Fe-sulfides showing a Fe-oxide rim (Fig. 2B). Zone II is composed of alternating, millimeter-wide

TABLE 1. REPRESENTATIVE ELECTRON MICROPROBE ANALYSES OF Fe-Mn OXYHYDROXIDES IN MARBLE BAR CHERT A458; Fe AND Ni SULFIDES IN BLACK CHERT PANO D-136–0; CARBONATES IN BLACK CHERT PANO D-136–0; AND HYDROMUSCOVITE IN KITTYS GAP CHERT KG 1

(A) Fe-Mn oxyhydroxides: A458

wt%	*in BIF*				in Qz vein	
Mg0	1.82	1.82	1.64	3.88	1.72	1.67
Al_2O_3	0.02	0.02	0.03	0.00	0.05	0.02
SiO_2	4.75	4.54	3.84	1.26	4.33	5.60
Cr2O3	0.03	0.06	0.00	0.00	0.00	0.00
CuO	0.08	0.00	0.02	0.19	0.10	0.00
ZnO	0.14	0.00	0.05	0.00	0.00	0.00
TiO_2	0.04	0.01	0.00	0.00	0.00	0.00
MnO	0.63	0.55	14.57	45.20	4.79	6.14
FeO	72.50	72.15	56.94	13.52	64.36	63.31
NiO	0.02	0.00	0.10	0.03	0.07	0.13
K_2O	0.00	0.01	0.08	0.59	0.00	0.04
CaO	0.13	0.05	0.36	0.48	0.30	0.25
Total	80.16	79.20	77.62	65.15	75.72	77.18

(B) Fe- and Ni-Sulfides: D-136–0

at%	Pyrite									Vaesite
S	66.57	64.02	66.68	65.61	67.14	66.85	66.48	66.23	66.39	67.26
Fe	33.30	28.72	32.11	30.63	31.65	32.33	32.46	32.81	32.67	0.74
Ni	0.00	0.41	0.66	0.90	0.64	0.28	0.09	0.26	0.28	30.72
Cu	0.03	0.05	0.14	0.00	0.10	0.06	0.01	0.01	0.05	0.01
Zn	0.00	0.04	0.01	0.01	0.02	0.00	0.03	0.01	0.03	0.05
As	0.00	0.15	0.24	0.80	0.30	0.35	0.86	0.57	0.47	0.52
Se	0.00	0.45	0.04	0.14	0.03	0.01	0.00	0.01	0.01	0.61
Pb	0.09	6.18	0.12	1.91	0.12	0.12	0.08	0.10	0.10	0.09
Total	99.99	100.02	100.00	100.00	100.00	100.00	100.00	100.00	100.00	100.00

(C) Carbonates: D-136–0

wt%	Dolomite		Calcite		
CaO	27.18	27.32	53.14	53.00	47.71
MgO	14.95	15.07	0.33	0.35	6.45
FeO	7.45	7.70	0.06	0.14	0.31
MnO	1.63	1.37	0.57	0.46	0.51
P205	0.33	0.35	0.69	0.82	0.56
F	0.10	0.00	0.09	0.00	0.00
	51.65	51.85	54.95	54.84	55.60

(D) Hydromuscovite: KG

wt%	Average of 78 analyses			
SiO_2	45.11	45.62	46.34	47.42
Al_2O_3	35.50	34.81	34.50	35.56
K_2O	6.44	10.09	9.32	9.12
MgO	0.48	0.63	1.44	0.65
Na_2O	0.37	0.46	0.36	0.38
Fe_2O_3	3.07	0.41	0.61	0.34
TiO_2	0.12	0.12	0.33	0.16
CaO	0.05	0.03	0.06	0.06
Cl	0.01	0.01	0.00	0.01
MnO	0.03	0.00	0.00	0.01
Total	91.17	92.16	92.97	93.72

Notes: Data in wt%. Electronmicroprobe analyses, Centre Camparis, Université Paris VI. Abbreviations: BIF—Banded Iron Formation; Qz—quartz.

iron-manganese oxyhydroxide (FeMnOH) and quartz bands (microbanded iron formations, micro–BIFs hereafter; Fig. 2A). The iron-rich bands are formed of skeletal goethite aggregates and euhedral rhombic-shaped phenocrysts of Fe-Mn oxyhydroxides (Fig. 2C). The phenocrysts have an inner euhedral core of vermicular textures and a heterogeneous composition of alternating bright and dark microbands. A euhedral overgrowth zone, containing traces of As and Ca is separated from the inner crystal by K-Al silicates (Fig. 2D). The focused ion beam transmission electron microscopy (FIB-TEM) investigations indicate that each microband is composed of nanoscopic filaments, each of them consisting of euhedral hematite crystals. The quartz bands between the FeMnOH rims contain numerous euhedral Fe-Mg oxide (magnesian-bearing magnetite or magnesioferrite) inclusions (Fig. 2E). Xenotime grains (Fig. 2F), rich in heavy rare earth elements (HREE) and Au-Pd-Fe-Cu-Ni alloys, occur interstitially with the FeMnOH. Zone III has a fine-grained homogeneous texture and is composed of microcrystalline quartz crosscut by millimeter-wide quartz veins, which contain FeMnOH with similar textures to those observed in the micro–BIFs and Ca-Mg carbonates which are partly or completely dissolved and replaced by FeMnOH (Fig. 2G). The microcrystalline quartz

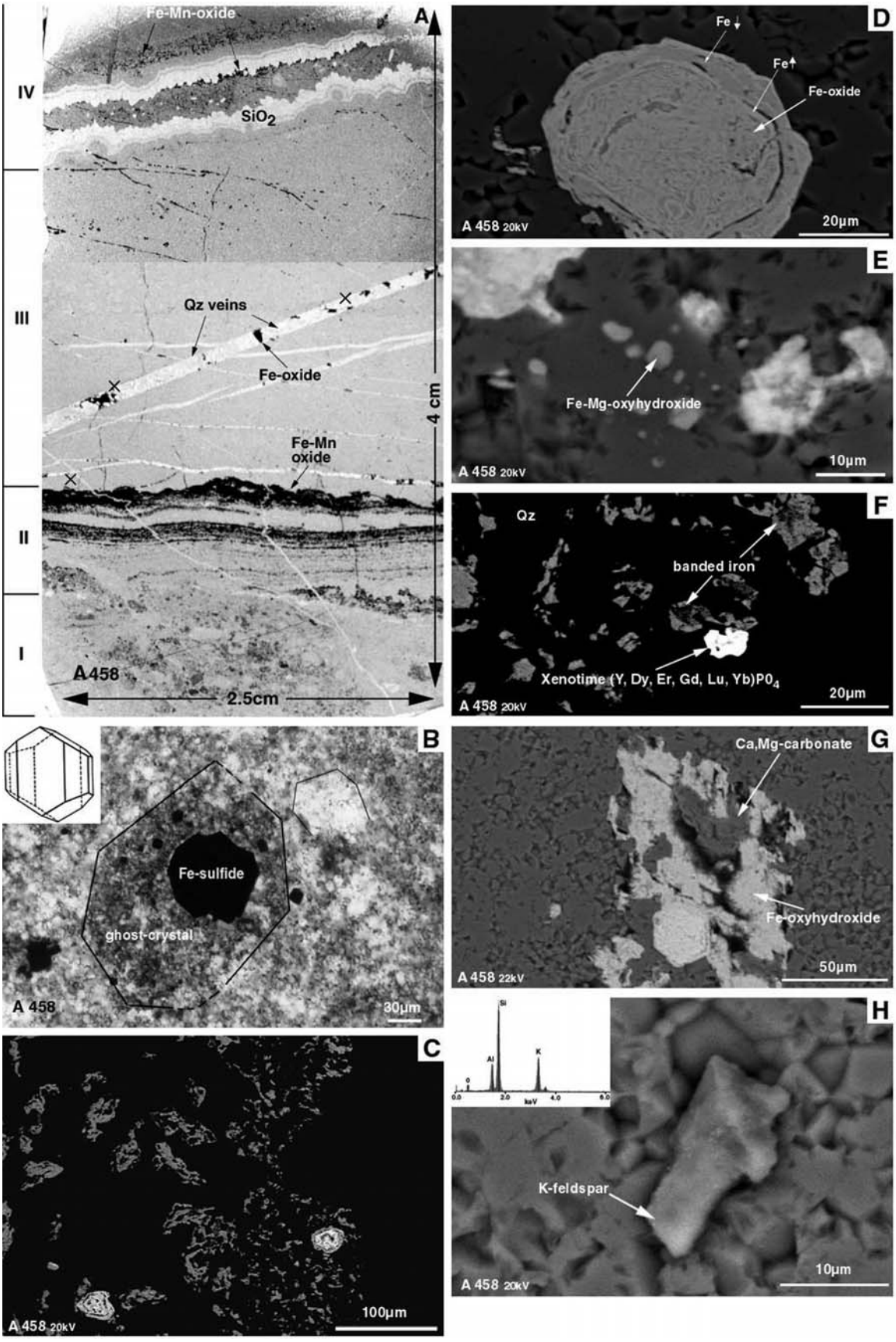

matrix of zone III contains micrometer-sized K-Al silicates (Fig. 2H), rarely barite and Ba-bearing mica, and occasionally, Fe-sulfides with similar textures to the FeMnOH.

Electron microprobe analyses and high-resolution SEM combined with Energy Dispersive X-ray Analysis (EDX) on these highly heterogeneous and porous samples show that the FeOH contains traces of MgO (~2 wt%), MnO (0.36–1.1 wt%), CaO (500–1700 ppm), and NiO (<400 ppm). Mn-oxyhydroxides contain 3–6 wt% FeO, NiO (<500 ppm), MgO (4 wt%), CaO, and K_2O (9000 ppm for both these elements). Locally, traces of Cu, Zn, and Ti (<200 ppm) were detected in Fe and Mn minerals. Microprobe analyses give totals <100 wt%, which can be related to volatile contents but also to the high porosity of these phases. It is noteworthy that the FeMnOH minerals do not have stoichiometric compositions (Table 1A).

Geochemistry

Based on their optical characteristics, chert sections of different color (zones I, II, III, Fig. 2A) were separated and analyzed by ICP-MS (Table 2). The three parts differ in chemical composition. The Fe-oxyhydroxide rich (FOH) micro–BIFs are about twice as enriched in Fe_{tot}, corresponding to Fe_2O_3 (Table 2) and MnO as the porphyritic part, and slightly richer in MgO. The micro–BIFs have K contents close to the detection limit of 0.05 wt%, which is related to the K-Al silicates intergrown with the FOH. The loss on ignition of 2.29 wt% reflects molecular and adsorbed water and other volatiles in FOH. The micro–BIFs are also richer in divalent iron (0.11 wt% FeO) compared to 0.055 wt% in the porphyritic part. The presence of divalent iron might be related to magnetite inclusions in the quartz between the FOH bands. The porphyritic part and the micro–BIFs have similar trace element contents of As, Co, Cr, Ni, Pb, Rb, and U (Table 2). The micro–BIFs are about twice as rich in Ba, Zn, and Y, whereas the porphyritic part is richer in Sb, Sr, Zr, and V. The chert precipitate (zone III, Fig. 2A) is depleted in all trace elements, except for Ge, Nb, Ta, and Zr (Table 2). Bulk sulfur content is low (0.085 wt%) and is related to the rare Fe-sulfides and tiny barite crystals in the chert precipitate. The Se/S ratio is 1.2×10^{-4} (Se: 100 ppb). The C1 normalized (Evensen et al., 1978) REE element patterns of the porphyritic part and the micro–BIFs are similar. They are enriched in HREE (heavy rare earth elements) and characterized by a positive Eu anomaly. The porphyritic part has slightly lower REE contents compared to those of the micro–BIFs. Zone III is essentially composed of microquartz and micro–K-Al silicates and has comparatively the lowest REE contents, with most REE giving values below the detection limit (Table 2).

Figure 2. (A) Thin-section scan of chert A458 showing the silicified precursor basalt part (zone I), and, at the top, the iron-manganese oxide precipitation (zone II) in contact with the silica precipitate that is crosscut by secondary quartz veins, which also contain Fe-Mn oxides. (B) Transmitted not polarized optical microscopic photograph: precursor mineral, now composed of microcrystalline quartz. Euhedral Fe-sulfide crystals are precipitated preferentially in these precursor relicts. (C) Scanning electron microscopy-backscattered secondary electrons (SEM-BSE) image: Skeletal Fe-Mn oxide containing euhedral Fe-Mn oxides; enlargements are shown in Figure 2D. (D) SEM-BSE image: euhedral Fe-oxides, with internal vermicular structure of heterogeneous chemical composition. The interface between the overgrowth and the internal crystal is made up of K-Al silicate. (E) SEM-BSE image: euhedral Fe-Mg-oxide (magnetite or magnesioferrite) inclusions in quartz interstitial to the Fe-Mn oxyhydroxide bands. (F) SEM-BSE image: HREE–rich (heavy rare earth element) xenotime in Fe-Mn oxyhydroxide bands. (G) SEM-BSE image: Ca-Mg carbonate replaced by Fe-Mn oxyhydroxides. (H) SEM-BSE image: subhedral K-feldspar (compare Energy Dispersive Spectroscopy [EDS] spectrum in inset) intergrown with microquartz

NORTH POLE CHERT–BARITE UNIT–DRESSER FORMATION (PANO D-136–0)

Mineralogy

The PANO D-136–0 sample is a compositionally homogeneous black chert. Microscopic crosscutting veins are filled with quartz. Pull-apart structures indicate extensional tectonic deformation during syn- or post-chert formation. Transmitted light microscopy shows that, prior to silicification, the rock had a brecciated texture (Fig. 3A). White and dark, subhedral to euhedral former crystal shapes are filled with microcrystalline quartz (Fig. 3B). Abundant organic matter occurs dispersed as filaments in the chert matrix or as oval inclusions in silica (Figs. 3C and 3D). The chert matrix hosts numerous K-Al-silicate crystals (5 μm) that are in some cases palagonite, according to FEG-SEM (Fig. 3E). Euhedral dolomite and calcite (Figs. 3F and 3G; Table 1C), Sm-Yb-Cl bearing apatite, xenotime, anhedral florencite, native gold, and Ti-oxides were also found (Figs. 3H and 3I). Spherulitic Fe-sulfides (<2 μm) occur as clusters in carbonates (Fig. 3F), where they replace subhedral to euhedral minerals and occur along the grain boundaries of microcrystalline quartz (Figs. 3J, 3K, and 3M). The Fe-sulfide nanospherules contain internal compartmentalized voids (Fig. 3L). Weblike Fe-sulfides are intergrown with sphalerite that hosts arsenopyrite inclusions (Figs. 3N and 3O). Galena occurs as inclusions in Fe-sulfides. The weblike Fe-sulfides contain trace amounts of Pb (0.03–7.37 at%), Ni (0.03–6.57 at%), As (0.17–1.55 at%), Cu (0.2 at%), Zn (up to 0.069 at%), and Se (up to 0.51 at%). Vaesite (NiS_2) contains, on average, 0.67 at% Se, 0.575 at% As, 0.81 at% Fe, up to 0.05 at% Zn, and 0.02 at% Cu (Table 1B). The carbonates include Mg-calcite containing ~0.5 wt% MnO and 7000–8200 ppm P_2O_5 and dolomite containing ~7 wt% Fe, 1.5 wt% Mn, and ~3500 ppm P_2O_5 (Table 1C).

Geochemistry

This black chert has a low total iron content (Fe_{tot} as Fe_2O_3: 0.27 wt%) with ~50% divalent Fe (0.13 wt%, Table 2). Sulfur and Se are 0.14 wt% and 0.67 ppm, respectively, giving a Se/S ratio of 4.8×10^{-4}. Selenium is incorporated in Fe- and Ni-

TABLE 2. BULK ROCK GEOCHEMISTRY OF CHERTS AND CHERT PARTS

Lithology	A section Tower Formation				Kittys Gap		Dresser Formation		
protolith	A 458 Bulk	A 458 I porphyric chert basalt	A 458 II BIF (FOH) BIF (Mag) precipitate	A 458 III white chert precipitate	KG 5 white chert	KG 6 black chert	D-136–0 black chert black shale	PANO C 85a white chert precipitate	PANO C 85b black chert black shale
					(pyroclastic sediments)				
SiO_2 (wt%)	94.26	91.89	83.91	99.21	92.36	96.28	98.79	99.4	96.26
Al_2O_3	0.19	0.42	0.16	<L.D.	5.51	2.63	0.27	<L.D.	0.24
Fe_2O_3	3.52	5.89	12.49	0.18	1.59	0.78	0.24	<L.D.	0.43
MnO	0.16	0.34	0.64	<L.D.	<L.D.	<L.D.	<L.D.	<L.D.	<L.D.
MgO	0.24	0.29	0.39	<L.D.	<L.D.	<L.D.	<L.D.	<L.D.	<L.D.
CaO	<L.D.	<L.D.	<L.D.	<L.D.	<L.D.	<L.D.	<L.D.	<L.D.	0.21
Na_2O	<L.D.	<L.D.	<L.D.	<L.D.	<L.D.	<L.D.	<L.D.	<L.D.	<L.D.
K_2O	<L.D.	<L.D.	0.05	<L.D.	1.59	0.78	0.05	<L.D.	<L.D.
TiO_2	<L.D.	<L.D.	<L.D.	<L.D.	0.28	0.09	<L.D.	<L.D.	<L.D.
P2O5	<L.D.	<L.D.	<L.D.	<L.D.	<L.D.	<L.D.	<L.D.	<L.D.	0.13
PF	0.79	1.58	2.29	<L.D.	<L.D.	<L.D.	0.41	0.39	1.38
Total	99.16	100.41	99.93	99.3	99.74	99.78	99.76	99.79	98.65
FeO	0.1	0.055	0.11	n.a.	n.a.	n.a.	0.13	n.a.	n.a.
S	0.085	n.a.	n.a.	n.a.	n.a.	n.a.	0.14	n.a.	0.39
CO_2	0.15	n.a.	n.a.	n.a.	n.a.	n.a.	0.58	n.a.	1.63
Corg	0.01	n.a.	n.a.	n.a.	n.a.	n.a.	0.14	n.a.	n.a.
H_2O+	0.56	n.a.	n.a.	n.a.	n.a.	n.a.	n.a.	n.a.	n.a.
$H_2O–$	0.05	n.a.	n.a.	n.a.	n.a.	n.a.	n.a.	n.a.	n.a.
Se (ppm)	0.1	n.a.	n.a.	n.a.	n.a.	n.a.	0.67	n.a.	n.a.
As	51.2	6.75	5.67	2.21	1.29	1.647	14.2	16.59	36.63
Ba	52.9	35.9	56.1	26.1	61.04	47.75	40.1	40.82	127.7
Be	<L.D.	<L.D.	<L.D.	<L.D.	<L.D.	<L.D.	<L.D.	<L.D.	<L.D.
Bi	<L.D.	<L.D.	<L.D.	<L.D.	<L.D.	<L.D.	0.12	0.25	0.46
Cd	<L.D.	<L.D.	<L.D.	<L.D.	<L.D.	<L.D.	1.07	<L.D.	1.95
Ce	0.86	1.03	0.56	0.29	14.6	12.95	1.15	0.58	6.65
CO_2	2.95	2.89	3.37	0.86	0.34	0.55	14	0.33	3.3
Cr	<L.D.	9.8	9.1	<L.D.	14.25	14.79	7.6	<L.D.	8.90
Cs	<L.D.	<L.D.	<L.D.	<L.D.	0.971	0.56	0.35	<L.D.	0.51
Cu	12.6	<L.D.	<L.D.	<L.D.	8.03	69.36	11.4	<L.D.	20.71
Dy	0.19	0.16	0.33	0.03	1.46	0.97	0.09	0.07	1.03
Er	0.15	0.15	0.23	0.02	0.87	0.52	0.05	0.04	0.57
Eu	0.05	0.05	0.08	<L.D.	0.49	0.38	0.03	0.02	0.28
Ga	0.4	0.99	0.56	0.34	9.01	4.33	0.46	0.23	0.8
Gd	0.15	0.13	0.2	<L.D.	1.44	1.08	0.09	0.06	1.01
Ge	1.26	1.16	1.08	1.18	2.08	2.09	0.85	0.89	0.91
Hf	<L.D.	0.07	<L.D.	0.04	1.65	1.01	0.1	<L.D.	0.12
Ho	0.04	0.04	0.08	<L.D.	0.29	0.18	0.02	0.02	0.22
In	<L.D.	0.26	0.26	0.15	<L.D.	<L.D.	0.06	0.18	0.31
La	0.45	0.52	0.26	0.10	7.37	6.27	0.57	0.35	4.47
Lu	0.03	0.04	0.08	<L.D.	0.13	0.07	0.01	0.01	0.07
Mo	0.93	<L.D.	<L.D.	<L.D.	<L.D.	<L.D.	0.77	78.91	1569
Nb	<L.D.	0.27	0.11	0.13	3.73	1.51	0.17	<L.D.	0.28
Nd	0.4	0.45	0.26	<L.D.	6.84	6.09	0.51	0.27	3.62
Ni	15.3	23.4	25.4	<L.D.	<L.D.	7.42	42	37.81	577.9
Pb	2.44	2.67	2.26	<L.D.	4.08	5.6	10	10.50	16.911
Pr	0.1	0.12	0.07	<L.D.	1.79	1.56	0.14	0.06	0.89
Rb	0.68	0.64	0.65	<L.D.	30.31	15.46	2.16	<L.D.	1.58
Sb	2.31	2.68	1.58	1.06	2.31	2.257	<L.D.	<L.D.	15.34
Sm	0.1	0.11	0.09	<L.D.	1.46	1.255	0.12	0.04	0.79
Sn	0.94	0.71	<L.D.	<L.D.	2.57	9.48	<L.D.	0.97	2.2
Sr	3.08	5.9	0.6	<L.D.	11.32	7.12	<L.D.	<L.D.	13.17
Ta	<L.D.	0.03	<L.D.	0.02	0.35	0.15	0.02	<L.D.	0.02
Tb	0.03	0.02	0.04	<L.D.	0.23	0.17	0.02	<L.D.	0.16
Th	<L.D.	0.11	<L.D.	<L.D.	2.19	1.37	0.32	<L.D.	0.28
Tm	0.02	0.03	0.05	<L.D.	0.14	0.07	0.01	0.01	0.08
U	0.07	0.13	0.1	<L.D.	0.57	0.40	0.13	0.35	15.81
V	1.87	7.2	4.6	<L.D.	42.89	23.69	3.5	<L.D.	20.41
W	0.11	<L.D.	<L.D.	<L.D.	2.36	1.34	0.07	0.16	0.84
Y	1.72	1.47	2.9	0.19	9.02	5.33	0.47	0.51	8.55
Yb	0.18	0.24	0.43	0.02	0.89	0.48	0.04	0.05	0.47
Zn	13.2	19.4	40.5	<L.D.	<L.D.	49.69	373	<L.D.	80.69
Zr	1.25	2.94	1.64	1.83	68.81	56.94	3.89	2.22	5.63
LaN/YbN	1.749	1.51	0.43	3.05	5.84	9.22	9.06	4.78	6.65

Notes: Analyses Service d'Analyse des Roches et Minéraux–Centre de Recherches Pétrographiques et Géochimiques (SARM–CRPG), Nancy, France. Abbreviations: BIF—Banded Iron Formation; FOH—Iron OxyHydroxides; L.D.—lower limit of detection; Mag—magnetite; n.a.—not analyzed. Major element data in wt%, trace element data in ppm.

sulfides (Table 1B). The presence of CO_2 (0.58 wt%) is related to Mg-Fe-Mn carbonates (Figs. 3F and 3G), and the organic carbon (0.14 wt%) is related to the organic matter embedded in microcrystalline quartz (Fig. 3D). High Zn contents of 373 ppm reflect the presence of sphalerite. Trace metals, such as As, Ni, Cu, Bi, Mo, Pb, and Cd, are incorporated in the Fe-Ni-Zn-sulfide structures (Table 1B). The C1-normalized REE pattern is slightly fractionated and depleted in HREE compared to LREE (light rare earth elements). A negative Eu and a positive Tm anomaly has been also noted.

NORTH POLE APEX BASALT FORMATION CHERT (PANO C-85)

Mineralogy

Chert PANO C-85 comprises a white and a black zone, each of which have a distinct mineralogy (Fig. 4A). Thin section observations reveal that a diffuse microcrystalline quartz vein system overprinted a previously formed chert. The white zone represents a part of the quartz vein system that contains mostly microquartz (Fig. 4B). Microscopic pull-apart structures, filled with relatively coarser-grained quartz, indicate that these veins were formed during an early extensional event. The black part has a complex mineralogical composition. Micrometer-sized Fe-oxides are abundant, and they exhibit different morphologies. (1) There are clusters of crystallites that pseudomorph mineral shapes that existed prior to silicification (Fig. 4C). The crystallites occur either as micro-ring–shaped structures or as spherules (Figs. 4D–4F). The spherules and ring-shaped structures are associated with K-Al silicates (K-feldspar?). (2) There are crystallites that are some tenths of a micrometer in size or occur as large subhedral to euhedral Fe-oxides showing heterogeneous agglomerated internal textures (Fig. 4G). These Fe-oxides contain $CaSO_4$ (possibly $+H_2O$) with traces of Cr. EDX analyses show that subhedral Fe-oxides contain V and As. (3) There are poikilotopic Fe-oxides of a heterogeneous composition (Fig. 4H) that contain inclusions of xenotime with traces of REE and W (Fig. 4I), as well as barite (Fig. 4J). In the black zone, micrometer-sized chalcopyrite occurs in interstitial and microcrystalline quartz. Furthermore, two types of poorly crystallized phases were observed: porous (with round holes), poorly crystallized, Si-rich phases, containing high amounts of Ca, Ba, and S, possibly indicating the presence of gypsum (anhydrite) and barite (Figs. 4K and 4L); and multielement (K-Al-Si-Ti-V-P-As-S-Sr-Ca-Pb-Ba) amorphous phases that sometimes include Fe-oxide in exsolution (Fig. 4M). Subhedral K-feldspar is rare.

Geochemistry

The white and black zones of sample PANO C-85 were analyzed separately (Table 2). The black zone has similar Al_2O_3 and Fe_2O_3 contents to those of the black chert PANO D-136–0. This zone hosts the highest P_2O_5 contents, at 0.13 wt%. Phosphorous occurs either as phosphates or in poorly crystallized multielement phases (Fig. 4I). The sulfur content of this black zone is twice that measured in the black chert PANO D-136–0. It is related to the presence of Ca-sulfates (gypsum or anhydrite) or barite (128 ppm Ba), rather than sulfides. The CO_2 content is three times higher than that in the white chert zone. It reflects the presence of carbonates. The most common base metals are Mo and Ni (at 1570 ppm and 578 ppm, respectively), which are more abundant than in the black chert PANO D-136–0, by a factor of ten.

The white zone is depleted in all elements compared to the black zone. However, As, Ba, Ni, and Pb abundances are as high as in the black chert PANO D-136–0. The REE patterns of the black and white zones are similar. They are LREE enriched (Fig. 5). However, the white zone is REE depleted by a factor of 10, in comparison to the black zone. Both zones show a slight negative Ce anomaly, which is more pronounced in the black than in the white part (Fig. 5A).

KITTYS GAP CHERT–PANORAMA FORMATION (KG 1)

Mineralogy

Sample KG 1 is composed of submillimeter- to millimeter-thick black and white laminae (Fig. 6A). Sedimentary structures indicative of formation in a tidal environment include channels, varying and bimodal current directions, and flaser-linsen bedding (de Vries, 2004). The major components of sample KG 1 are microcrystalline quartz (85–90 vol%) and hydromuscovite. The white and black laminae show different textures and grain size that were determined prior to silicification; however no difference in the respective mineralogies has been observed. The

Figure 3. Microphotographs of chert PANO D-136–0. (A) Thin-section scan. (B) Plane polarized light microphotograph showing the brecciated texture of the precursor black shale; dark precursor minerals are now composed of microquartz and sulfide clusters. (C) Organic matter dispersed in the microquartz matrix. (D) Field Emission Gun Scanning Electron Microscopy (FEG-SEM) photograph: NO_3-etched microquartz grain with organic matter. (E) Scanning electron microscopy-backscattered secondary electrons (SEM-BSE) image: subhedral K-Al silicate, probably K-feldspar, in cryptocrystalline quartz. (F) Plane polarized light microphotograph showing opaque mineral clusters (Fe-sulfides) on Mg-carbonate. (G) SEM-BSE image euhedral, zoned Mg-carbonate; the central zone contains traces of Cr and Mn. (H) SEM-BSE image: euhedral, HREE–bearing (heavy rare earth element) apatite in quartz matrix. (I) Florencite in quartz matrix. (J) Plane polarized light and reflected light microphotographs: spherulitic sulfide clusters replace euhedral precursor mineral. (K) Plane polarized light microphotograph: spherulitic sulfide clusters composed of nanospherules. (L) SEM-BSE image showing details of sulfide clusters. They are composed of Fe-sulfides with internal void structures. (M) Fe-sulfide in the form of alignments of spherules. (N) Massive Fe-sulfides intergrown with arsenopyrite and sphalerite. (O) Fe-sulfide with alternating more massive and weblike zones.

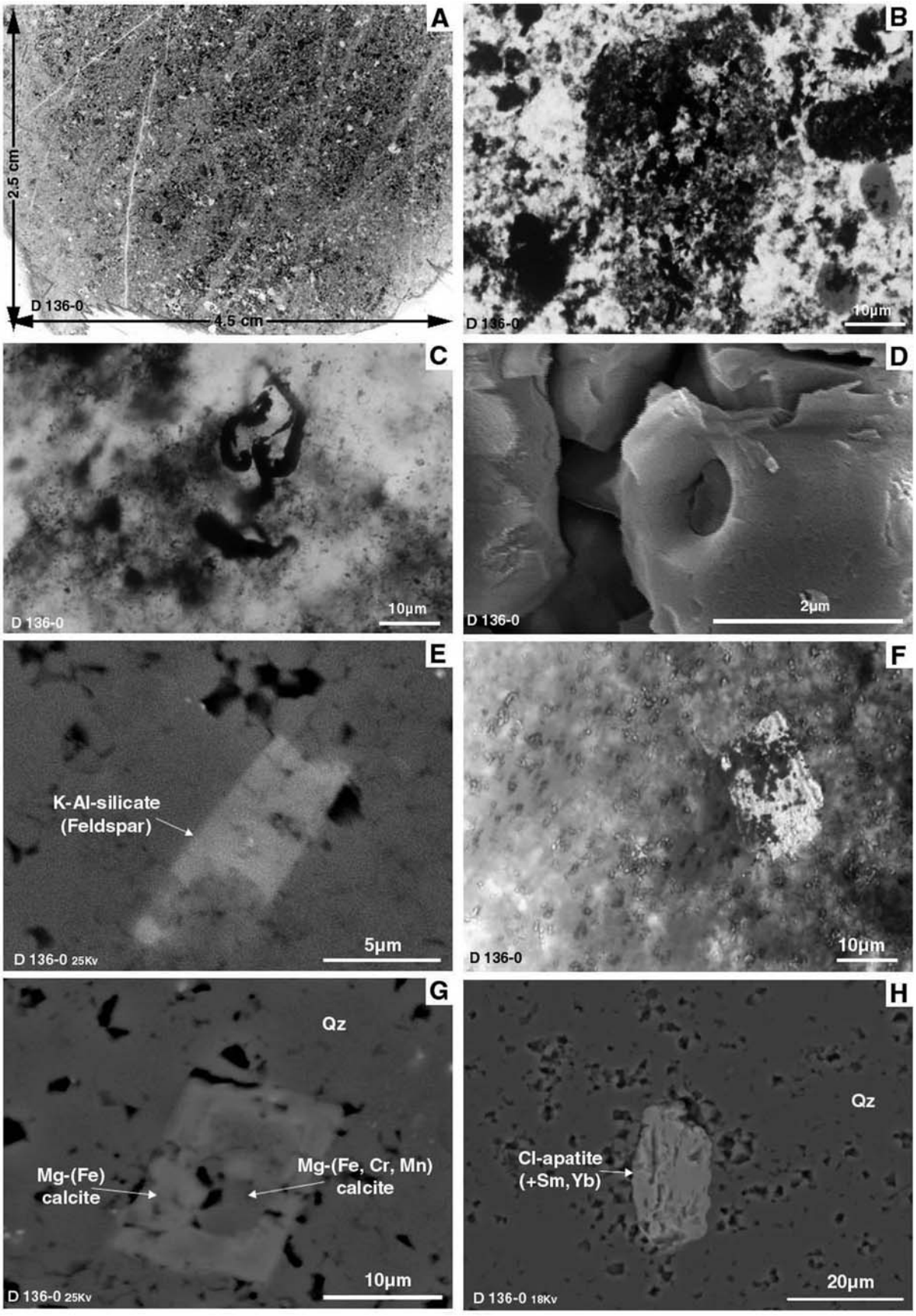

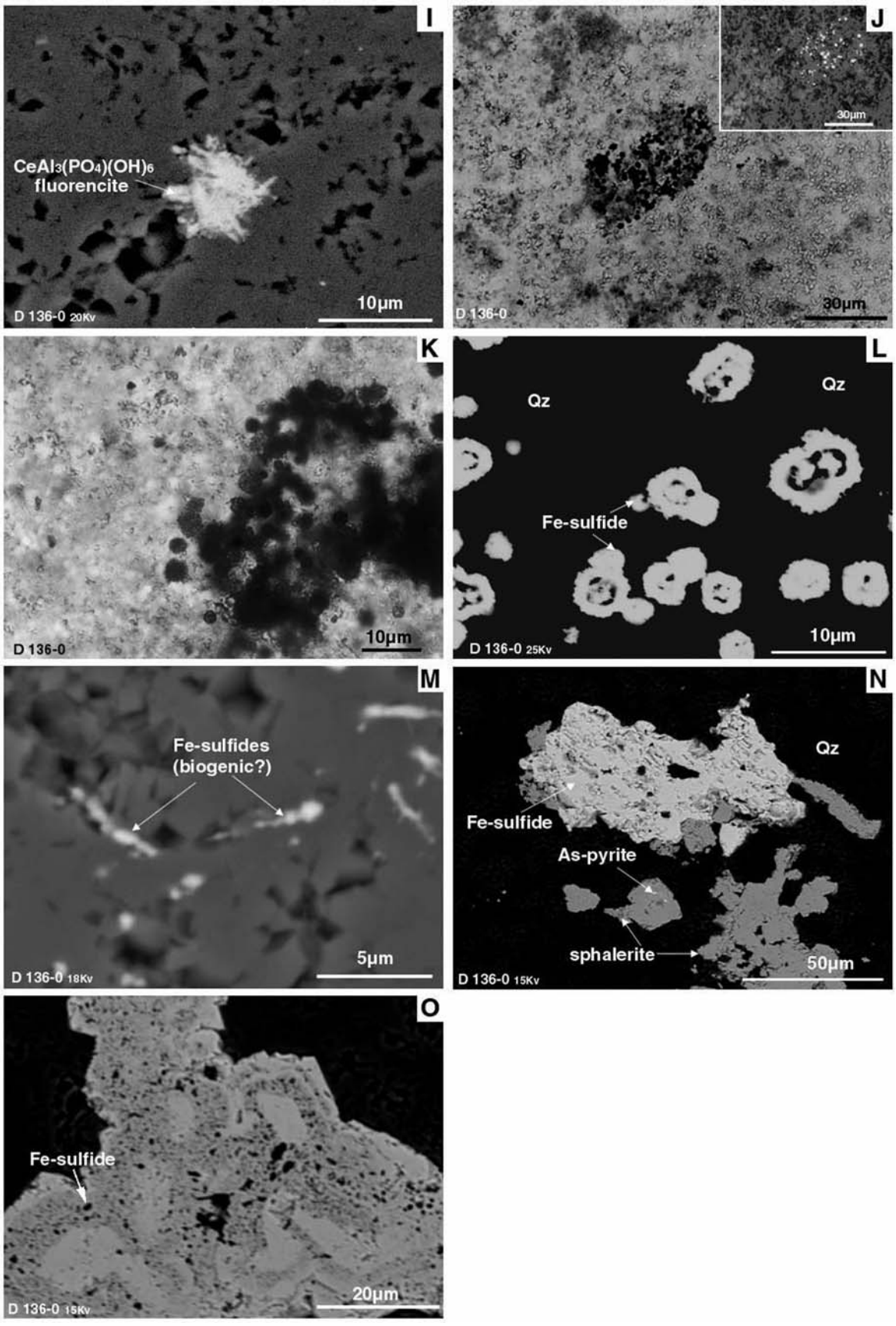

black laminae are fine grained and contain fewer porphyroclasts, which are now ghost clasts, than the white laminae (Fig. 6B). Three types of ghost clasts have been distinguished: (1) euhedral to subhedral crystal shapes, replaced by hydromuscovite and outlined by nanometer-sized Ti-oxide spherules (Fig. 6C); (2) euhedral crystals (100–300 μm) replaced by hydromuscovite (Fig. 6D); and (3) euhedral ghost crystals with aggregates of hydromuscovite and Ti-oxides intergrown with quartz (Fig. 6E). These ghost crystals are interpreted to be either Ti-bearing mica, K-feldspar, or amphibole. Anhedral aggregates of hydromuscovite and minor quartz, outlined by Ti-oxide spherules, could represent glass shards or mineral debris (Fig. 6F). Accessory monazite, florencite, and zoned and corraded zircons are more abundant in the white laminae (Figs. 6G and 6H). Poorly crystallized phases composed of Zr-Ti-REE and U are rare (Fig. 6D). Organic matter occurs as clusters around the volcaniclasts or as delicate mats on laminae surfaces (Fig. 6I) and also as detrital particles (Westall et al., this volume). Hydromuscovite has variable chemistry, containing traces of MgO (0.38–1.44 wt%), Na_2O (0.22–0.79 wt%), Fe_2O_3 (=Fe_{tot}: 0.02–3.07 wt%), TiO_2 (0–0.52 wt%), CaO (0.03–0.11 wt%), Cl (up to 0.03 wt%), and MnO (up to 0.5 wt%; Table 1D). KG 1–6 lamina was analyzed for N and C by nuclear reaction analysis (Rouchon et al., 2005), because it contains a silicified microbial mat at the interface with the KG 5 lamina. Hydromuscovite contains N contents between 0.013 and 0.112 at% in KG 1–5 lamina and between 0.054 and 0.087 at% in KG 1–6 lamina. Carbon amounts range from 0.01 to 0.60 at% in lamina KG 1–5 and from 0.1 to 0.5 at% in KG 1–6 lamina. The C/N atomic ratio ranges from 0.08 to 20.9 and varies with the C concentration (Rouchon et al., 2005).

Geochemistry

The black and the white chert laminae in sample KG 1 are compositionally different. The white laminae have twice the abundances of Al_2O_3, Fe_2O_3, and K_2O in the black part, owing to a higher abundance of hydromuscovite. Three times higher Ti contents indicate also that Ti-oxides are more common in the white than in the black laminae. The poorly crystalline, multi-element phases are a second Ti carrier (Fig. 6D). Only the trace elements, such as V (Ti-oxides), Rb, and Sr (hydromuscovite) related to the above-mentioned minerals, are enriched in the white laminae. Copper, Zn, Ni, and Sn are enriched in the black laminae, whereas the white laminae are relatively richer in Zr, Y, W, Nb, Ta, and Ba. The REE patterns show a slight fractionation of LREE compared to the HREE. Black and white laminae have the same LREE abundances, but white laminae are richer in HREE (Fig. 5A).

DISCUSSION

Most of the Archean cherts are considered to be derived from silicification of either orthochems, carbonaceous and volcaniclastic sediments (Lowe and Worrell, 1999; Walsh and Lowe, 1999; Lowe 1999), or mafic and ultramafic rocks (de Wit et al., 1982; Appel et al., 2001; Myers, 2001). Cherts in banded iron formations are generally attributed to chemical precipitation (Bolhar et al., 2004, Bau and Dulski, 1996) or to a combination of exhalation and chemical sedimentation (Gross, 1980; Lydon, 1984; Kimberley, 1989).

Many of the replacement cherts show sedimentary structures, such as fine laminations, wave-rippled strata, carbonaceous matter influx prior to silicification (e.g., cherts from Hoggenoeg and Kromberg Formations, Barberton Greenstone Belt, South Africa: Lowe and Worrell, 1999; de Vries, 2004; the Kittys Gap chert from the Coppin belt and North Pole Chert–Barite Unit, Pilbara Craton, Western Australia; Nijman et al., 1998; de Vries, 2004; Dunlop, 1978; Barley, 1993; Dunlop and Buick, 1981). In the Pilbara craton, the depositional environments are mainly interpreted as low-energy marine coastal-lagoonal submarine to subaerial or partly evaporitic environments. Depositional depths are estimated at less than 100 m (Buick and Barnes, 1984; Lowe and Worrell, 1999; de Vries, 2004). In contrast, deep-water settings and high-temperature hydrothermal environments similar to modern MOR settings were suggested for the Marble Bar Greenstone belt (Kato and Nakamura, 2003) and the North Pole Chert–Barite Unit (Kitajima et al., 2001). As sedimentary or magmatic features are well preserved, all authors agree that silicification is an early synsedimentary diagenetic and/or exhalative process, occurring at the water-sediment interface (Knauth and Lowe, 1978; Lowe and Byerly, 1999; Lowe, 1999). However, post-depositional silicification by circulating hydrothermal fluid has also been proposed (de Wit et al., 1982; Barley, 1993; Buick and Barnes, 1984; Paris et al., 1985; Duchac, 1986; Lowe and

Figure 4. Microphotographs of chert PANO C-85. (A) Scan of thin section with white and black parts of the chert. (B) Thin section of the white part showing several generations of silicification. (C) Scanning electron microscopy-backscattered secondary electrons (SEM-BSE) image: iron-oxide clusters precipitated on precursor crystal. (D) SEM-BSE image: detail of Fe-oxide cluster and the corresponding Energy Dispersive Spectroscopy (EDS) spectrum. It has to be noted that K-Al-silicate is always present. Fe-oxides show voids and spherulitic agglomeration texture. (E) SEM-BSE image: clusters of Fe-oxide with voids; in foreground, spherulitic Fe-oxide. (F) SEM-BSE image: spherulitic Fe-oxide texture. (G) SEM-BSE photograph: euhedral Fe-oxide showing spherulitic Fe-oxides at its lower rim. Its heterogeneous texture might reflect that it was formed by recrystallization of spherulitic oxides. (H) SEM-BSE image: poikilotopic Fe-oxide. The corresponding EDS spectrum shows that these oxides contain traces of V and As. (I) SEM-BSE image: xenotime crystals rich in REE (rare earth elements; see corresponding EDS spectrum) precipitated as secondary product at the edge of Fe-oxides. (J–M) SEM-BSE images: poorly crystalline, gel-like, silica-rich phases and their corresponding qualitative EDS spectra: (J) SEM-BSE image: crystals of barite in poorly crystallized silica-rich phase. (K–L) SEM-BSE images: Silica gel–like phase containing Ca-Ba and S, probably reflecting the presence of nanometer-sized crystals of barite and gypsum. (M) SEM-BSE image: silica phase with high amounts of K and Al, traces of V and Ti, as well as distinct crystals of Fe-oxides.

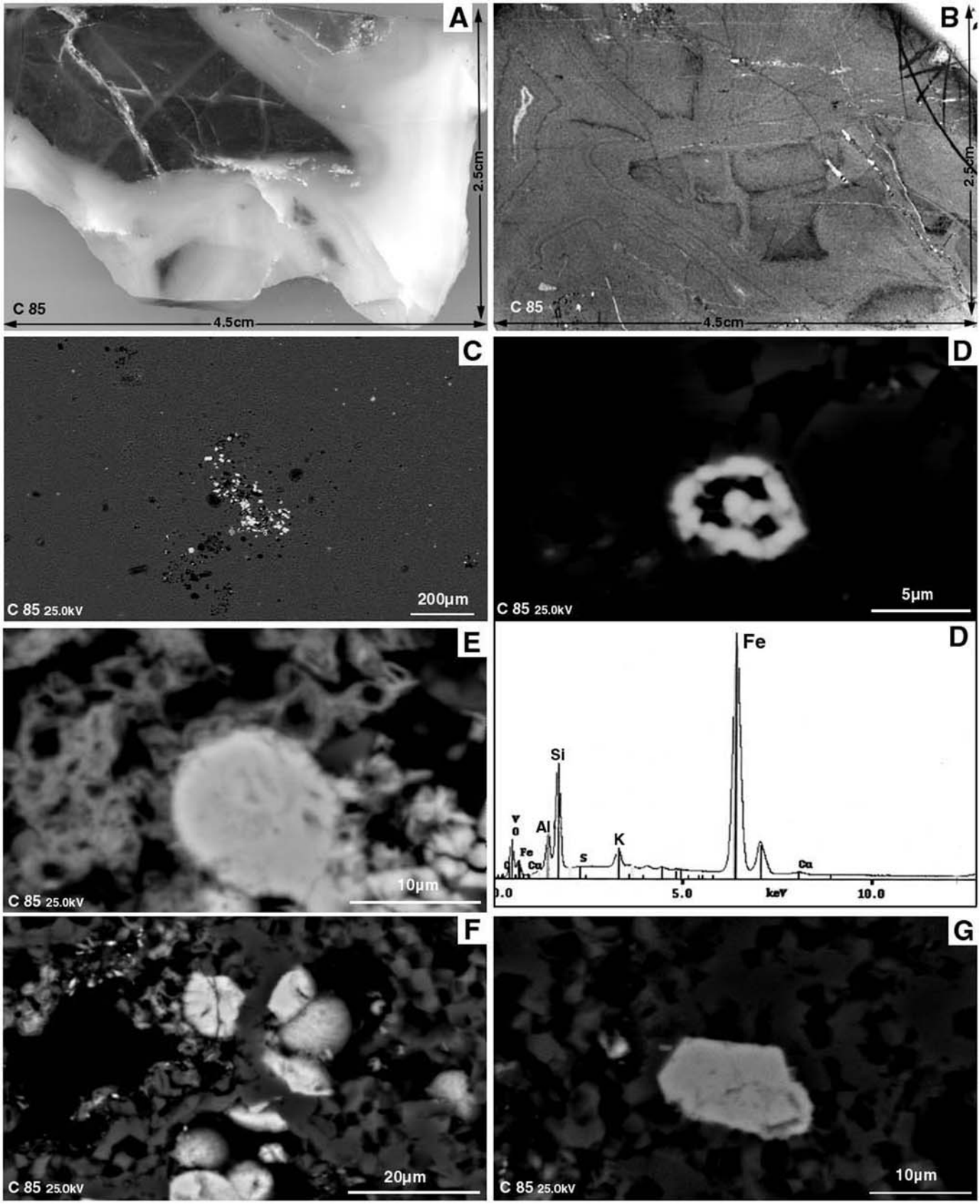

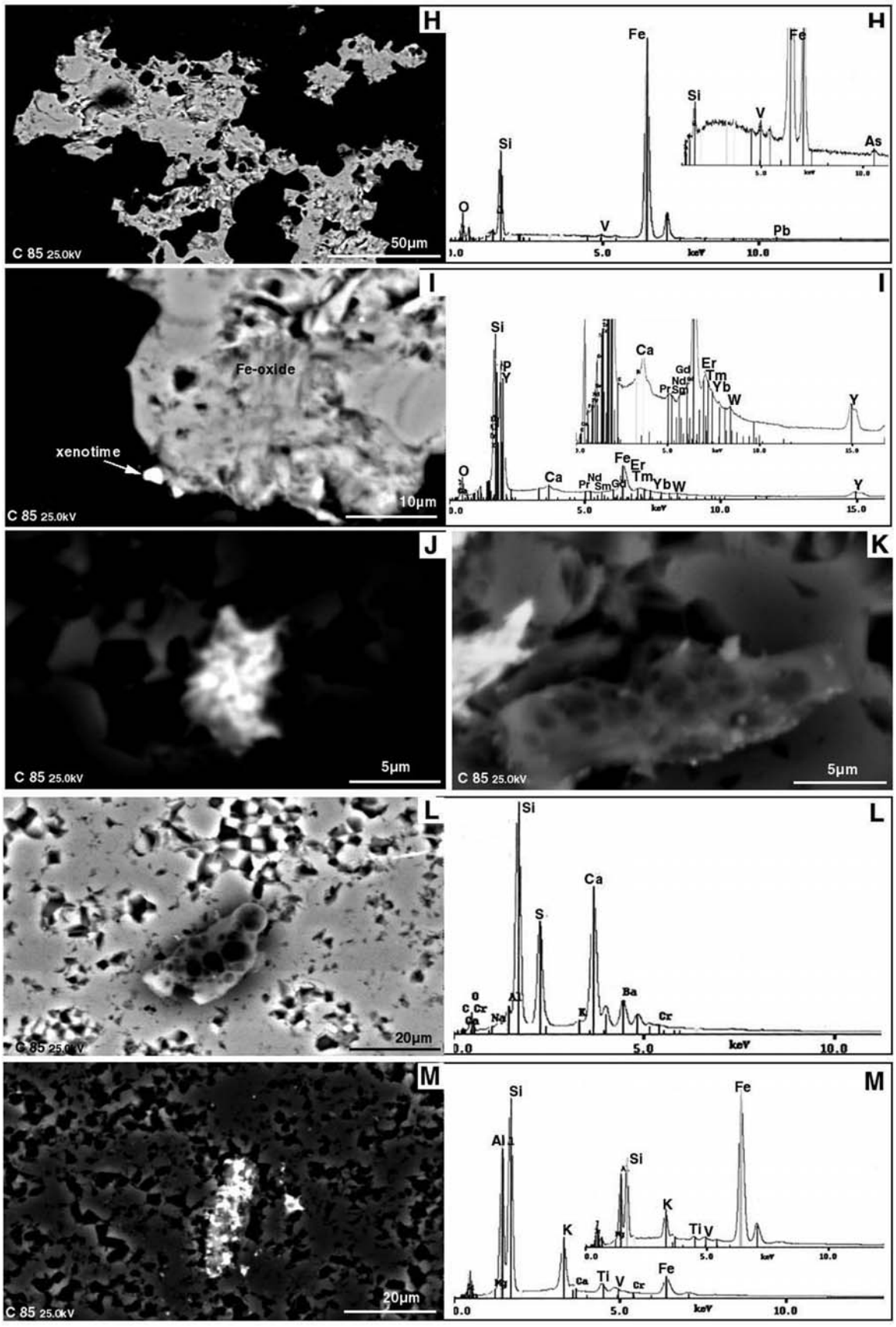

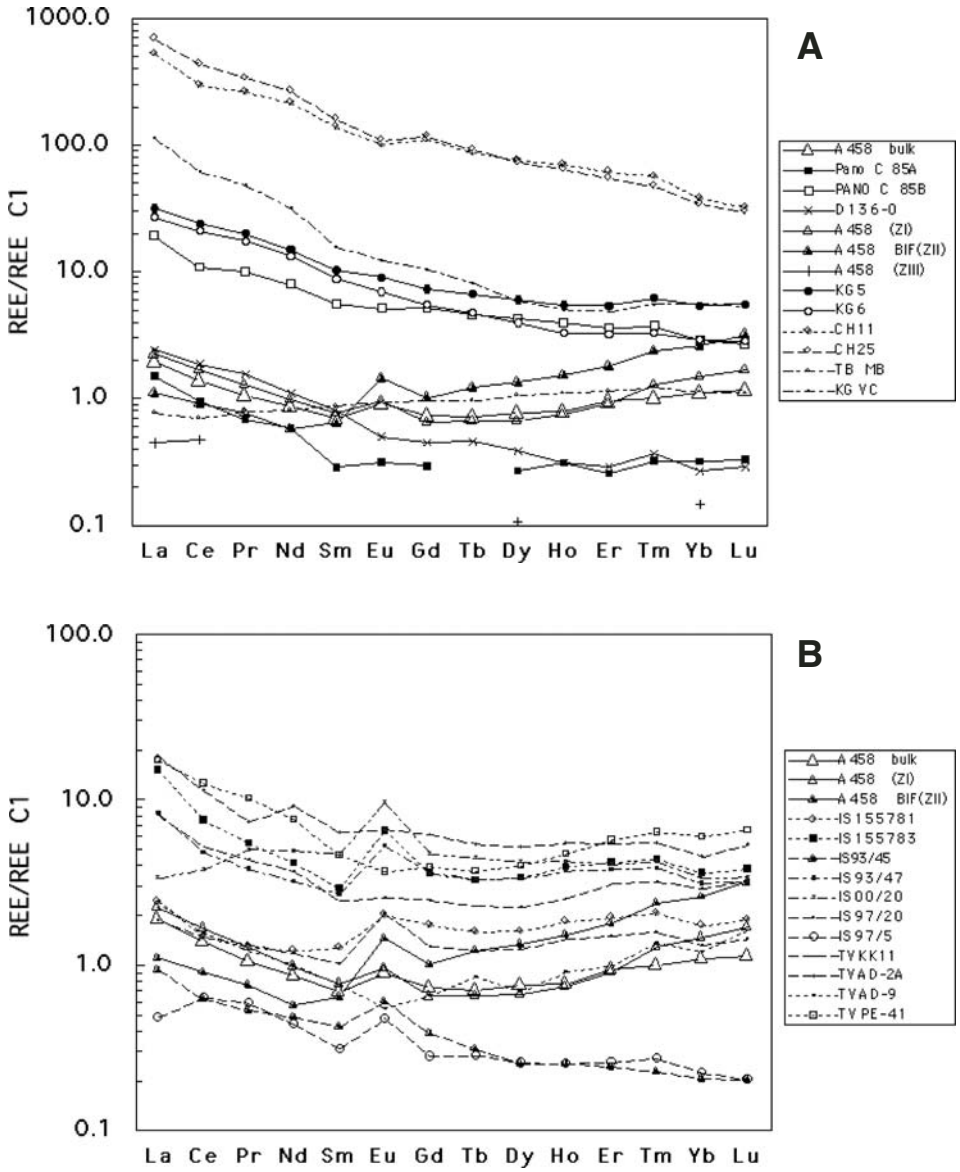

Figure 5. C1 normalized REE (rare earth element) patterns (normalization values after Evensen et al., 1978) for the studied samples from the Pilbara complex, and for comparison, for other samples. (A) A 458 bulk: A section Towers Formation, ZI (zone I)—porphyritic part (precursor: basalt); ZII (zone II)—micro–BIF (Banded Iron Formation); ZIII (zone III)—microcrystalline quartz intergrown with K-Al silicates; PANO C-85 A—white part; PANO C-85 B—black part; PANO D-136–0—black chert; KG 1–5—white chert lamina of chert KG 1; KG 1–6: black chert part of chert KG 1; TB MB—tholeiitic basalt, Marble Bar, Towers Formation (from Kato and Nakamura, 2003); KG VC—Rhyodacite, Kittys Gap (de Vries, 2004); CH11, CH25—black shales from the Nuitang Formation, South China (Lower Cambrian) (Orberger et al., 2005b). (B) Comparison of the A458 zone I and II (micro–BIF) to TV (Transvaal Supergroup): BIF Transvaal Supergroup (Bau and Dulski, 1996) and IS—BIF Isua Supracrustal Belt, Greenland (Bolhar et al., 2004).

Byerly, 1999; Hanor and Duchac, 1990). The origin of the silica has been related to either (1) hydrothermal discharge from deep-seated magmatic systems, based on combined field observations and fluid inclusion data (e.g., de Vries, 2004); (2) silica-rich, downward-circulating ocean water (Holland, 1973; Siever, 1992; de Ronde et al., 1997); (3) alteration of volcaniclastic material (Lowe and Byerly, 1999); or (4) a combination of these processes.

The geodynamic settings of the cherts studied here are well constrained, and hydrothermalism is considered, at least in part, as one of the major processes that controlled silicification (e.g., Sugitani, 1992; Van Kranendonk et al., 2001; Nijman et al., 1998), although silica-rich seawater circulation might also have been an important process during silicification of the Kittys Gap sediments (de Vries, 2004). Marble Bar chert A458 comes from

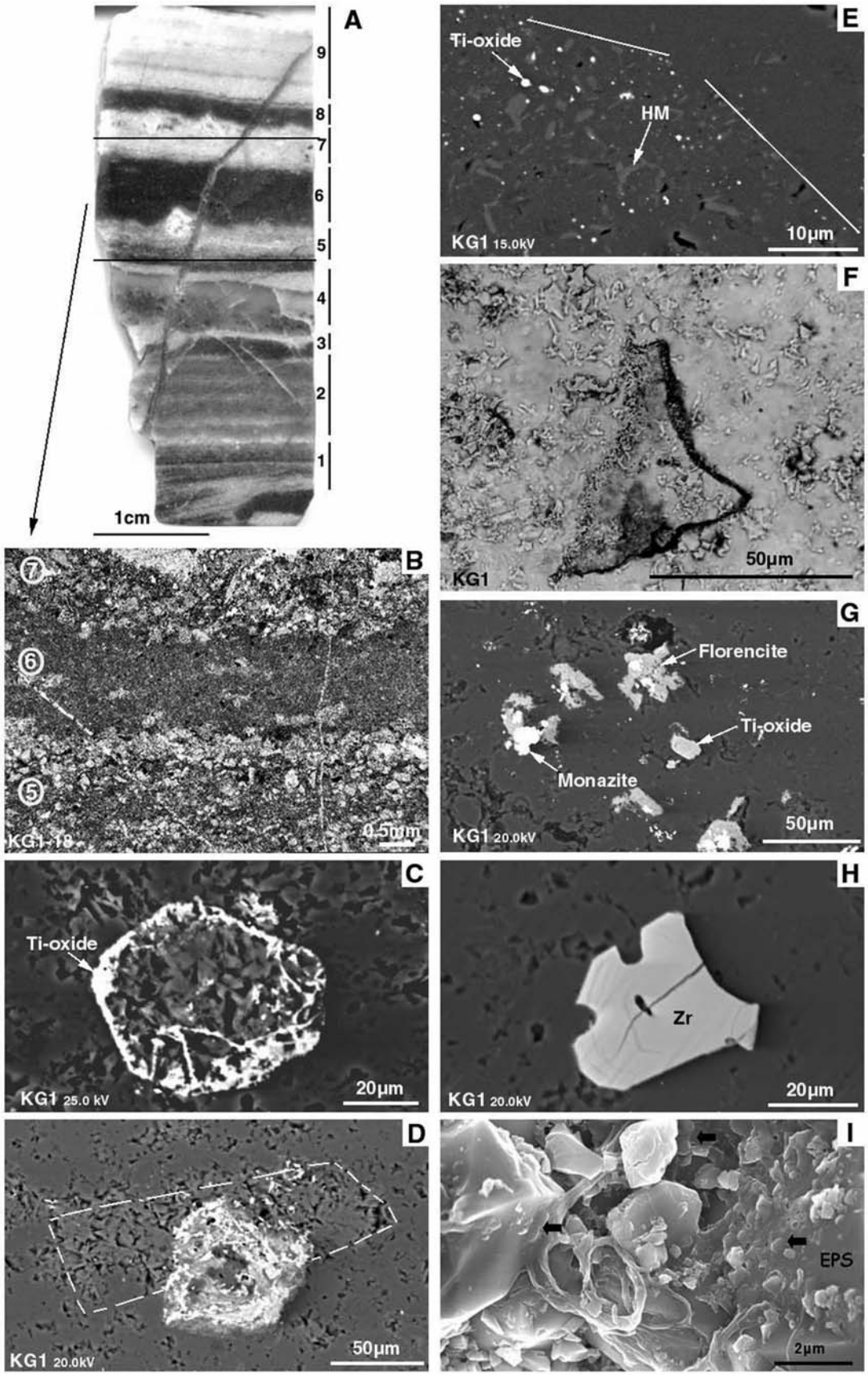

the A-section of the Towers Formation. Cherts from this section are interpreted as precipitates derived from a high-temperature hydrothermal solution emanating from a MOR (Kato and Nakamura, 2003). Mantlelike xenon anomalies observed in this chert (Pinti et al., 2001a) have been interpreted as contamination by mantle-derived pervasive fluid or, alternatively, produced by neutron capture reactions with Te, a rare element concentrated in hydrothermal-derived ores. The two chert samples PANO D-136–0 and PANO C-85 come from silica dykes of probable hydrothermal origin (Isozaki et al., 1999; Nijman et al., 1998; Ueno et al., 2004; Nijman et al., 1998). The Kittys Gap chert was deposited in a shallow water environment on top of rhyodacitic to rhyolitic rocks (de Vries, 2004). Our study shows that the physical, biological, and chemical conditions during silicification were controlled by the protolith mineralogy and chemistry and the nature of the fluid.

Hydrothermal Fluid-Basalt Interaction

In modern and Phanerozoic environments, banded iron or diffuse iron-oxide bearing cherts can be formed in coastal shallow-water settings accompanied by volcanic activity, as those of Papua–New Guinea (Tarasov et al., 1999), or at MOR, where Fe-Mn oxyhydroxides precipitate from hydrothermal plumes up to some distance from the hydrothermal vent (e.g., Grenne and Slack, 2003a). Biologically mediated precipitation of Fe was also suggested for BIFs (Nealson and Myers, 1990) and occurs in Phanerozoic shallow-water carbonate rocks (Préat et al., 2004).

Marble Bar chert A458 is partly characterized by porphyritic or volcaniclastic textures with euhedral to subhedral precursor minerals. The trace element composition of microquartz being pseudomorphous after such precursor minerals indicates that the dark quartz is rich in Fe, Mg, Ti, Ca, and Mn, whereas the bright transparent quartz is poor in mafic elements (Gallien et al., 2003). The texture, mineralogy, and mineral chemistry strongly favor a basaltic (volcaniclastic) protolith for the zone I of this chert.

Figure 6. Microphotographs of the chert from Kittys Gap (KG 1). (A) Thin-section scan showing alternating black and white chert bands with sedimentary textures. (B) Reflected light microphotograph of layers 5–7, as indicated in (A). (C) Scanning electron microscopy-backscattered secondary electrons (SEM-BSE) image: precursor mineral, probably biotite, with rims outlined by Ti-oxide; the precursor mineral is replaced by hydromuscovite and microquartz. (D) SEM-BSE image: precursor K-feldspar (as emphasized by dashed lines), now replaced by hydromuscovite in microcrystalline quartz matrix. (E) SEM-BSE image: a precursor mineral (amphibole?) (margin marked by the white line) is now composed of Ti-oxide and hydromuscovite and is intergrown with microquartz. (F) SEM-BSE image: precursor glass shard replaced by microquartz and outlined by microspherules of Ti-oxide. (G) SEM-BSE image: florencite and monazite intergrown with Ti-oxide in microquartz. (H) SEM-BSE image: Corroded zircon. (I) Field Emission Gun Scanning Electron Microscopy (FEG-SEM) image: silicified organic mats. EPS—extracellular polysaccharide.

The interface between the precursor basalt and the pure chert precipitate is marked by the precipitation of micro–BIFs, now composed of Fe-Mn oxyhydroxides and exhibiting stromatolite-like structures. These REE patterns are similar to those observed in the silicified basalt, but have higher REE abundance. This indicates a similar source and a similar fractionation process for these two zones. The presence of euhedral sulfides with textures similar to those of the later-formed vermicular Fe-oxides in the protobasaltic rock (zone I) and in the chert precipitate (zone III) indicates a reducing environment. The occurrence of Mg-carbonate relicts suggests that this environment was also alkaline. The magnetite or magnesioferrite inclusions in the silica bands intercalated with the Fe-Mn-oxyhydroxide bands indicate that the BIF was previously composed of magnetite and a reducing environment (see reaction [3] below). Metals such as Cr, Ni, Au, Pd, P, Y, and HREE coprecipitated with Fe-Mn oxides and may have been desorbed during later infiltration of low-temperature, oxidizing fluids. During this episode, magnetite was oxidized into hematite and Fe-Mn oxyhydroxides. Since the Fe-Mn oxyhydroxides contain traces of Mg and Ca, we suggest that part of these elements derived from the dissolution of carbonate precursors and were incorporated into the hydroxide structure. The following reactions illustrate the pathway to the presently observed phases. Mg-carbonate and silica formation might be the result of a classical Urey reaction.

$$CaSiO_3 + CO_2 = CaCO_3 + SiO_2. \quad (1)$$

Magnetite can form through hydrolysis or silicification, according to reactions (2) and (3).

$$3Fe_2SiO_4 + H_2SiO_4 = 2Fe_3O_4 + 4SiO_2 + H_2. \quad (2)$$

$$3Fe_2SiO_4 + 2H_2O = 2Fe_3O_4 + 3SiO_2 + 2H_2. \quad (3)$$

Sulfide formation and simultaneous magnetite formation can occur during simple hydrolysis through reaction (4):

$$6FeS + 4H_2O = Fe_3O_4 + 3FeS_2 + 4H_2. \quad (4)$$

The REE patterns of this porphyritic chert part (zone I) and the micro–BIFs differ clearly from that of the North Pole Dome black cherts and from the silicified volcaniclastic sediments of Kittys Gap. Both have a strong positive Eu anomaly and the HREE are enriched compared to LREE, leading to La_N/Yb_N ratios of 0.43 for the micro–BIFs and 1.75 for the silicified basalt of zone I (Fig. 5A, Table 2). As chert A458 is intercalated with tholeiitic basalts, a representative analysis (Kato and Nakamura, 2003) was plotted in Figure 5A. The chert is REE depleted by about five times compared to the abundances in tholeiitic basalt of the Towers Formation and differs by the presence of the positive Eu anomaly. We interpret the REE pattern of zone I and II of chert A458 as being the result of high-

temperature hydrothermal fluid–tholeiitic basalt interaction, which led to leaching of Eu from plagioclases of the oceanic basaltic crust. The absence of a Ce anomaly confirms the conclusion that silicification of the basalt occurred under fO_2 conditions equal to the hematite-magnetite buffer.

For comparison, representative data of BIFs from the Isua Supracrustal Belt (often associated with mafic and ultramafic rocks as in the Archean Amitsoq gneiss complex), from the Island of Akilia (Bolhar et al., 2004), and from the Penge and Kuruman iron formations, Transvaal Supergroups, are plotted in Figure 5B (Bau and Dulski, 1996). The Isua rocks all have similar patterns showing a positive Eu anomaly but slightly lower HREE contents (La_N/Yb_N of 1.4–4.7) compared to the A458 micro–BIFs (zone II) and the basaltic silicified protolith of zone I. The Isua BIFs are all rich in mafic minerals (pyroxenes and amphiboles). However, the considerable amounts of carbonates and apatite in the BIFs might be responsible for the lower HREE composition (Bolhar et al., 2004). With the exception of the rocks from the Isua Supracrustal Belt, all other samples were interpreted as being replacement cherts and not chemical sediments (Bolhar et al., 2004). However, BIFs from the Transvaal Supergroups have been interpreted as precipitates from a mixture of seawater and hydrothermal fluids (Bau and Dulski, 1996). Figure 5B shows that the Transvaal samples have no or only slight positive Eu-anomalies, but all are enriched in HREE. This could be due to a low hydrothermal fluid contribution to seawater. The case studied here represents both a basaltic rock replacement (A458 zone I) and a chemical (possibly biochemical) precipitate (A458 zone II, micro–BIFs) at the contact with the precursor basalt. The pronounced positive Eu anomaly, thus, is interpreted to reflect intensive fluid-basalt interaction whereby Eu was leached from the basaltic plagioclase and was subsequently adsorbed onto FeMnOH surfaces during BIF precipitation. Zone III of chert A458 is a pure precipitate from a silica-rich, K-Al-S-Ba–bearing aqueous solution, likely the residual fluid left after crystallization of the micro–BIFs. With the exception of La, Ce, and Yb, all other REE were retained during micro–BIF precipitation (Table 2, Fig. 5A).

Later oxidizing fluids infiltrated along fractures and oxidized magnetite to Fe-Mn-oxyhydroxides, dissolved carbonates, and replaced them pseudomorphically by Fe-Mn oxyhydroxides. Au-Pd-Ni-Cr alloys as well as xenotime are concentrated in the BIF Zone II. Hematitized, originally magnetite-bearing BIFs occur in the Isua Supracrustal Belt, where the hematitization was related to meteoric, low-temperature, oxygenic, alkaline fluid infiltration after the metamorphic event into penetrative zones (Myers, 2001). On the other hand, hematite-goethite deposits can be primary deposits formed in modern and Phanerozoic low-temperature, submarine, hydrothermal environments (<100 °C; Uyeda, 1987; Herzig et al., 1988; Juniper and Fouquet, 1988; Grenne and Slack, 2003a). Assuming the magnetite precursor for the FeMnOH, the following reactions can be proposed:

$$2Fe_3O_4 + H_2O = > 2\ Fe_2O_3 + H_2. \quad (5)$$

$$2FeO + 2H_2O = > 2\ FeOOH + H_2. \quad (6)$$

Sulfide, the second precursor mineral can be transformed by:

$$2FeS_2 + Fe_3O_4 + 4O_2 = > Fe_2O_3 + 2SO_4 + 4H^+. \quad (7)$$

The vermicular microscopic textures and filamentous, clustered nanotextures of the hematite might be related to microbial activity. Similar nanotextures were observed for ferrihydrite formed by the activity of Fe-oxidizing bacteria growing in near-neutral pH groundwaters (Banfield and Zhang, 2001). A further argument supporting microbial activity is the observed nonstoichiometry of the Fe-Mn oxyhydroxides (Tebo et al., 1997). However, according to FIB-TEM investigations, the nonstoichiometry may result from high nanoporosity in the nanofilaments and clusters. On the other hand, it is well known that microbial activity participates in the precipitation of Fe deposits (Grenne and Slack, 2003a). Thus, it is possible that microbes could have been active during the formation of the micro–BIFs. Mineralized filaments, similar in size and form to biofilm-forming bacteria, have been observed in Fe-smectite deposits near deep-seated hydrothermal vents. These microbial structures are similar to the features observed in the laminar overgrown zone on K-Al silicates at the interface of the Fe-oxide grains (Fig. 2C).

Nitrogen and carbon were analyzed by nuclear reactions in different mineral phases of the chert A458. Nitrogen was mainly found concentrated in the Fe-Mn oxyhydroxides in an unknown chemical form, possibly ammonium (Gallien et al., 2003). The C/N atomic ratio in the Fe-Mn oxyhydroxides ranges from 2.3 to 19.4, which is very similar to the C/N ratio measured in organic matter preserved in modern or Phanerozoic marine sediments (e.g., Rau et al., 1987; Muzuka et al., 1991) or starved marine bacteria in oceanic and MOR sediments (Takano et al., 2004). Previous N isotopic analyses of this chert (Pinti et al., 2001b; K. Hashizume, 2005, personal commun.) showed the occurrence of a main N component released at low temperature (600–800 °C) during stepped combustion. This component has a $\delta^{15}N$ value ranging from 6.7 ± 1.6 to 7.4 ± 2.4‰. New N isotopic analyses on BIF separates of the zone II show an N component released mainly at 800 °C and having a $\delta^{15}N$ of 7.6 ± 0.5‰. This isotopic ratio is identical to that of Phanerozoic marine sedimentary organic matter of +6 to +7‰ (Sweeney et al., 1978). The nitrogen isotopic composition of organic matter in modern environments is controlled by denitrification ($NO_3^- \rightarrow N_2$). During denitrification, ^{14}N returns preferentially to the atmosphere, leaving NO_3^- enriched in ^{15}N in oceanic water. As NO_3^- is the main nitrogen-bearing nutrient, marine organisms record its isotopic signature and are systematically enriched in ^{15}N by ~ +6‰ relative to the atmosphere. The N isotopic ratios measured in A458 could have recorded an Archean N cycle dominated by oxide species as that observed in Phanerozoic ages, or, alternatively, could have been added successively during postdepositional alteration (Fig. 4 *in* Pinti et al., 2001b). The first hypothesis seems not to be supported by

the available data (Beaumont and Robert, 1999; Pinti et al., 2001b; Pinti and Hashizume, 2001) that suggest, to the contrary, an Archean N cycle dominated by fixation of reduced species such as NH_4^+.

The second hypothesis is linked to the timing of the oxidizing fluid entry, which has not yet been determined. It can be speculated that intensive modern weathering would have affected the entire sample and not only selective areas. However, numerous sulfides are still present. Nitrogen can be introduced in cherts by modern weathering, but this component is always released at combustion temperatures between 100 and 450 °C (Pinti et al., 2001b, 2003; van Zuilen et al., 2005), and it shows much larger positive or negative isotopic fractionations (from –13 to +20‰; Pinti et al., 2001b) than that observed in this case. The N component released at 800 °C has possibly been added later, but probably before silicification of the sample. Further investigation is needed to determine the timing of oxidation and the consequences that it has on the interpretation of the N chemical signature.

Hydrothermal Fluid–Black Shale Interaction

Black cherts have many types of occurrences as (1) thin layers within cross-bedded volcaniclastic sandstone; (2) lenticular units; (3) fine laminations, drapes, and/or flaser layers between and within cross-beds in shallow marine to lagoonal sediments (Lowe and Byerly, 1999); and (4) irregular veinlets and dykes as, for example, seen in the Msauli chert, Onverwacht Group, Barberton Greenstone Belt (Hofmann, 2004), or at the North Pole Dome (Nijman et al., 1998; de Vries, 2004). These dykes were interpreted either as representing reinjected carbonaceous sediments from the subsurface (Lowe and Byerly, 1999) or as being related to hydrothermal activity and associated with tectono-metamorphic processes (Nijman et al., 1998; Hofmann, 2004). Our black chert samples (PANO D-136–0 and C-85) were taken from dykes, suggesting a direct association with hydrothermal activity (Nijman et al., 1998). However, our studies show that the two black cherts are not simply hydrothermal silica precipitates but rather silicified brecciated sediments. The brecciated precursor texture is still visible in all three analyzed chert parts (the black of the PANO D-136–0 and the white and black parts of PANO C-85), and all parts show identical REE patterns. The PANO C-85 black chert is enriched in REE by about ten times compared to the white part. The black chert PANO D-136–0 is REE depleted by ~8 times, compared to the black part of chert PANO C-85 (Fig. 5A). The main difference between the two chert samples is the presence of a more pronounced negative Ce anomaly in the black zone of chert PANO C-85, indicating that silicification occurred under, at least, slightly oxidizing conditions (Fig. 5A). The white zone has formed later because white microquartz veins crosscut the black zone. This indicates clearly that the more pronounced negative Ce anomaly of the black zone is related to the first silicification event. It can be speculated that Fe-oxide clusters were derived from sulfides, as observed in PANO D-136–0. However, barite and gypsum grains were found interstitial to the microquartz, favoring oxidizing conditions during silicification.

The PANO D-136–0 black chert is enriched in sulfides, organic matter, and carbonates and does not show a negative Ce anomaly. It was, thus, formed under reducing and alkaline conditions. The PANO C-85 chert contains multielement, poorly crystallized, porous phases, which were not found in the PANO D-136–0 sample. These amorphous textures might be the result of rapid silicification that conserved traces of the metal-charged silica gel–like phase. Such phases might represent the precursor from which inorganic colloidal particles precipitated (Williams and Crerar, 1985). Similar structures were observed in jaspers from the Lokken ophiolite (Grenne and Slack, 2003b). One of the striking similarities between the two PANO cherts is the texture and location of micrometer-sized Fe-oxide and Fe-sulfide clusters. Compartmentalized sulfide structures, such as those observed as clusters on the precursor minerals, are also typical for sulfur bacteria in modern environments (Boetius, 2004). Light $\delta^{15}N$ values (–7.4 ± 1.0‰ and –1.3 ± 1.6‰ respectively) measured in these rocks would support the hypothesis of biological activity at the time of their formation (Pinti et al., 2001b). Preliminary FIB-TEM investigations combined with electron energy loss spectroscopy (EELS) show that nitrogen is, in part, related to nanometer-sized films around microquartz grains (Wirth and Orberger, 2005, personal commun.). This indicates that N emplacement is clearly contemporaneous with silicification and not related to a later fluid event. In situ S and Fe isotopic measurements would be necessary to clearly identify a biological influence on the formation of these minerals.

Did hydrothermal fluids cause the silicification? There are arguments in favor of and against this hypothesis. No positive Eu anomaly, which would clearly indicate a hot hydrothermal fluid contribution, was observed in the black cherts (Douville et al., 1999; Fig. 5A). However, if we compare our results with REE patterns of Archean marine shales that have not been altered by hydrothermal fluids but were deposited by seawater, we should observe a negative Eu anomaly (Condie, 1991; Grenne and Slack, 2003b). The absence of this negative Eu anomaly in our PANO cherts can, thus, be interpreted as reflecting low-temperature hydrothermal fluid alteration. Low water-rock interaction does not necessarily produce a well-pronounced positive Eu anomaly as observed in high T hydrothermal fluids (e.g., Grenne and Slack, 2003a; Orberger et al., 2005b). REE analyses of another black chert from the Dresser Formation, sampled at the root of a silica dyke and within pillowed basalts (sample Pi-47–00; Pinti et al., 2003), show a well-defined positive Eu anomaly and a REE pattern identical to those observed in MOR effluents and chimney sediments (Mills and Elderfield, 1995). A hydrothermal fluid origin is also supported by the mineralogical and metal associations characteristic for submarine hydrothermal environments found in chert PANO D-136–0 (sphalerite, galena, chalcopyrite, pyrite, and Ni-sulfides), PANO C-85 (barite, gypsum, Fe-oxides) REE data from the black shale deposit of the Lower Cambrian Nuitang Formation in South China have been plotted together with our data in Fig-

ure 5A. These shales were deposited in shelf settings and were clearly infiltrated by hydrothermal fluids as proven by sulfur isotopic compositions of the sulfides and sulfates and by fluid inclusion data (Steiner et al., 2001; Orberger et al., 2005b). They are associated with cherts and phosphorites (Horan et al., 1994; Steiner et al., 2001; Orberger et al., 2005b). Several features observed in PANO D-136–0 and C-85 are similar to metal-rich black shales (e.g., from the Upper Devonian Selwyn Basin, Yukon, Canada: Horan et al., 1994; Orberger et al., 2003; or from the Lower Cambrian of southern China: Steiner et al., 2001). Specific features of these rocks are: (1) the association of metals of contrasting geochemical behavior and typical of hydrothermal environments, such as Zn, Fe, Pb, Fe, Se, and As in PANO D-136–0; (2) Se/S ratios in the order of 1×10^{-4} found in the sulfide-rich chert PANO D-136–0, which is in the same order of magnitude as that of BIF–bearing chert A458 and typical of hydrothermal volcanogenic environments (Auclair et al., 1987; Huston et al., 1995; Orberger and Alleweldt, 1994); (3) the presence of abundant organic matter; (4) the clastic-brecciated precursor texture; and (5) the sulfide morphologies and assemblages as well as the carbonate, phosphate, and sulfate mineralogy. The REE patterns of the black cherts PANO D-136–0 and C-85 are identical to those of the Lower Cambrian black shales (Steiner et al., 2001; Orberger et al., 2005b), but the absolute concentrations are lower by a factor of ~150–200 (Fig. 5A), which is interpreted as a dilution effect produced by the silicification. These black shales, although infiltrated by hydrothermal fluids, do not show a positive Eu anomaly as would be expected and as observed in our samples. Indeed, they are even characterized by a slightly negative Eu anomaly (Orberger et al., 2005b).

The Archean, metal-rich black cherts from the Nichol Well, Roerbourne Megasequence, Pilbara, have been interpreted as black shale deposits in the vicinity of a hydrothermal vent (Sugitani et al., 2002). The Apex Basalt Formation, from which the PANO C-85 chert was obtained, contains well-preserved black shale deposits with sulfide nodules, which have been found by The Archean Biosphere Drilling Project (Nedachi, 2004). Extremely light carbon isotopic compositions up to –40‰ measured in these lithologies suggest the activities of metanothrophs in black shales (Nedachi, 2004). Interestingly, this latter feature is in agreement with light nitrogen isotopic compositions found in PANO C-85 ($\delta^{15}N$ of –1.3 ± 1.6‰) and PANO D-136–0 ($\delta^{15}N$ of –7.4 ± 1.0‰). These N isotopic signatures have been interpreted as the result of the metabolic activity of chemoautotrophic bacteria in the proximity of an Archean MOR (Pinti and Hashizume, 2001). With regard to the black shale precursor rocks, the depositional environment can, however, be constrained as a low-temperature, hydrothermal shallow-water setting.

As the black cherts investigated here were obtained from dykes, we suggest that the dyke-derived black cherts represent material that was entrained into the hydrothermal system during hydrofracturing and brecciation. In that case, two generations of organic matter would be present in these samples: (1) organic carbon (kerogenes) encapsulated in silica as relict organic matter from the black shales, and (2) organic matter that decayed during sulfurization and oxidation contemporaneous with the silicification event. The environment in the immediate vicinity of the vent could have been highly conducive to microbial activity. The Lower Cambrian mineralized black shale of the Niutang Formation exemplifies such a situation (Mao et al., 2002; Steiner et al., 2001). These black shales contain evidence for a sudden mass distribution of fossils during Cambrian explosion (the so-called Cambrian explosion; Conway Morris, 1989; Bergström, 1989). Abundant fauna and mats of sheathed sulfur bacteria were observed in adjacent sediments, whereas arthropods, sponges, and undetermined shelly remains occur in the unit itself (Steiner et al., 2001). In this example, hydrothermal seeps or vents were the mediators for promoting biocolonization of the shallow-water environments. In light of this discussion, (black) cherts with a black shale precursor must represent important targets in the search for evidence of early Archean life.

Seawater-Rhyodacitic Volcaniclastic Sediment Interactions

The 3.446 Ga Kittys Gap volcano-sedimentary deposits were deposited in a shallow-water environment where hydrothermal venting was active during or shortly after sedimentation (de Vries, 2004). Multiple silicification events produced different vein generations and silicified different parts of the sedimentary rocks. Although black and white laminae of sample KG 1 do not show a significant difference in mineralogy except for a higher abundance of hydromuscovite and Ti-oxides in the white laminae, the phyllosilicates seem to be responsible for the slightly higher HREE content compared to that found in the black laminae (Fig. 5A). LREE patterns are almost identical in the two types of laminae. When comparing the REE pattern of the black and white laminae to that of the underlying rhyodacitic rocks (KG-rhyodacite, Fig. 5A), we note that the latter show a slight negative Ce anomaly, indicating slightly oxidizing conditions during deposition. Furthermore, the rhyodacitic rocks are a factor of two higher in LREE but show identical HREE contents compared to the white laminae. It can, thus, be concluded that although Ti-oxides are abundant in the cherts and no sulfides are observed, slightly reducing conditions were likely the cause for the absence of the negative Ce anomaly. The silicifying environment was likely more acidic, resulting in preferential precipitation of K-mica over K-feldspar. These redox conditions were favorable for the growth of the microbial mats on sediment surfaces and around volcaniclastic particles, whose signatures are expressed as microfossils and $\delta^{13}C$ ratios of –22 to –30‰ (Westall, 2005, 2003; Westall et al., 2004; see also Westall et al., this volume). In certain horizons of the sediment, the fossilized microbial remains appear relatively degraded. Nitrogen found in hydromuscovite may have originated from the decay of organic matter during silicification and incorporation in the phyllosilicate structure as NH_4^+ replacing K^+. Systematic enrichment of Cu, Cr, and Zn in all laminae, compared to average rhyodacitic rocks, might indicate a slight hydrothermal influence during silicification.

The Role of Phosphates

Phosphorous is one of the most important biophile elements, and its chemical cycle is closely linked to that of oxygen, carbon, sulfur, nitrogen, and iron (Föllmi, 1990). In the Archean, phosphorous in cherts hosting possible traces of life could have originated from the decay of organic matter. Microbes could have obtained P, an important nutrient, from the bioalteration of phosphorous-containing volcanic particles. Phosphorous could also have been leached from P-bearing minerals during silicification or could have been introduced by seawater or hydrothermal fluids. The origin and significance of phosphates in Archean rocks has been a controversial subject since Mojzsis et al. (1996) interpreted the association of isotopically light carbon isotopic values of graphite and apatite in 3760 Ma rocks (interpreted as BIFs) from the Isua Supracrustal Belt as a potential biomarker. Fedo and Whitehouse (2002), on the other hand, showed that the BIF was not of sedimentary origin. Lepland et al. (2002) and van Zuilen et al. (2003) demonstrated that the apatite and graphite, respectively, had an abiogenic origin by showing that graphite was formed through thermal decomposition of siderite at 800 °C and that the REE pattern of apatite reflects a chemical precipitate.

The phosphate mineralogy of our samples can be used to reconstruct the protolith of cherts: LREE phosphates (monazite, florencite, apatite) seem to be more abundant in the rhyodacitic protoliths, as at Kittys Gap, whereas HREE phosphates (xenotimes) are more common in basaltic rocks as in the A458 zone I. HREE– (xenotime) and LREE–rich (apatite) phosphates are characteristic of black shale protoliths influenced by metal-rich exhalative fluids, as in chert PANO D-136–0. The Kittys Gap chert contains euhedral to subhedral phosphates (florencite, monazite) intergrown with the silica matrix, reflecting the chemical composition of the silicifying fluid or relict detrital minerals (zircons), whereas anhedral textures or fillings of interstitial pore space, such as florencite in the Kittys Gap chert, could be attributed also to postsilicification events. Further study of our samples that include cherts with abundant organic matter containing a higher content and a larger variety of abiogenic phosphate minerals, as well as cherts that are poor in organic matter, might provide valuable information for elucidating the origin of P-containing minerals, thus making an important contribution to the solution of the Archean phosphate controversy.

CONCLUSIONS

Micromineralogical and detailed geochemical studies of four early Archean chert samples show that characterization of their depositional environments contributes significantly to the understanding of their origins (protoliths) and of the physical, biological, and chemical conditions during silicification. The studied cherts were partially infiltrated by hydrothermal fluids. Three of the cherts had a sedimentary protolith. The black cherts PANO D-136–0 and PANO C-85 had a black shale precursor, whereas the white and black laminated chert from the Kittys Gap had a rhyodacitic volcaniclastic precursor. The PANO cherts, which were sampled from hydrothermal dykes, might represent entrained, brecciated sediments (black shales), which were silicified by hydrothermal fluids. For the Kittys Gap chert, the enriched Cu and Zn values in the black laminae might indicate a slight contribution from hydrothermal fluid infiltration. The geochemical signature of the A458 chert from the Towers Formation is a result of basalt-hydrothermal fluid interaction. With the exception of the chert PANO C-85, silicification of the studied samples occurred in all cases under reducing conditions. Mineral structures, such as Fe-sulfides infilling voids, Fe-oxides occurring as clusters, and vermicular Fe-Mn oxide structures composed of nanofilaments, which consist of aligned hematite nanoclusters, suggest that microbial activity may have influenced mineral formation. For the PANO and the Kittys Gap cherts, this microbial activity is likely contemporaneous with the silicification event. Additional arguments for the presence of life at the time of silicification are provided by C/N ratios, the $\delta^{13}C$ and $\delta^{15}N$ values, and the location of N in nanofilms around microquartz grains or incorporated in hydromuscovite structures as ammonium (Rouchon et al., 2005). The nanometer-sized, filamentous, clustered hematite in the micro–BIFs of A458 zone II is related to a postsilicification oxidizing fluid event.

APPENDIX

Details on the precision, detection limits and analytical procedures are available at http://www.crpg.cnrs-nancy.fr/SARM/index.html.

ACKNOWLEDGMENTS

DLP wishes to thank Drs. Maruyama, Isozaki, and Ueno for providing samples A458, PANO D-136-0, and C-85, together with geological information. This study was funded by the French national programs (CNRS [Centre National de la Recherche Scientifique] GDR [Groupe de Recherche]-Exobiologie, CNRS-PNP [Project National Planétologie], CNES [Centre National d'Etudes Spatiales]-Exobiology) and by the CNRS-UPS UMR-8148 IDES (Interactions and Dynamique des Environments de Surface) at Université Paris XI. We thank M. Fialin and F. Couffigal for helping with electron microprobe observation and A. Richard during FEG-SEM analysis. The comments and corrections of M. Walsh and A. Hoffmann greatly improved the paper.

REFERENCES CITED

Appel, P.W.U., Rollinson, H.R., and Touret, J.L.R., 2001, Remnants of an early Archaean (>3.75 Ga) seafloor, hydrothermal system in the Isua Greenstone Belt: Precambrian Research, v. 112, p. 27–49, doi: 10.1016/S0301-9268(01)00169-3.

Auclair, G., Fouquet, Y., and Bohn, M., 1987, Distribution of selenium in high-temperature hydrothermal sulfide deposits at 13 degrees North, East Pacific Rise: Canadian Mineralogist, v. 25, p. 577–587.

Banfield, J.F., and Zhang, H., 2001, Nanocrystals as model systems for pressure-induced structural phase transitions, *in* Banfield J.F., and Navrotsky, A., eds., Nanoparticles and the environment: Reviews in Mineralogy and Geochemistry, Volume 44: Washington, D.C., Mineralogical Society of America, p. 1–51.

Barley, M.E., 1993, Volcanic, sedimentary and tectonostratigraphy environments of the ~3.46 Ga Warrawoona Megasequence: A review: Precambrian Research, v. 60, p. 47–67, doi: 10.1016/0301-9268(93)90044-3.

Bau, M., and Dulski, P., 1996, Distribution of yttrium and rare-earth elements in the Pengeand Kuruman iron formations, Transvaal Supergroup, South Africa: Precambrian Research, v. 79, p. 37–55, doi: 10.1016/0301-9268(95)00087-9.

Beauchamp, B., and Baud, A., 2002, Growth and demise of Permian biogenic chert along northwest Pangea: Evidence for end-Permian collapse of thermohaline circulation: Palaeogeography, Palaeoclimatology, Palaeoecology, v. 184, p. 37–63, doi: 10.1016/S0031-0182(02)00245-6.

Beaumont, V., and Robert, F., 1999, Nitrogen isotope ratios of kerogens in Precambrian cherts: A record of the evolution of atmosphere chemistry?: Precambrian Research, v. 96, p. 63–82, doi: 10.1016/S0301-9268(99)00005-4.

Bergström, J., 1989, Metazoan evolution around the Precambrian-Cambrian transition, *in* Simonetta, A.M., and Conway Morris, S., eds., The early evolution of Metazoa and the significance of problematic taxa: Cambridge, UK, Cambridge University Press, p. 25–34.

Boetius, A., 2004, Linking Biosphere to Geosphere: Anoxic microbial habitats at continental margins: 2nd Swiss Geoscience meeting, Lausanne, Switzerland: Abstracts, v. 1, p. 91.

Bolhar, R., Kamber, B.S., Moorbath, S., Fedo, C.M., and Whitehouse, M.J., 2004, Characterisation of early Archaean chemical sediments by trace element signatures: Earth and Planetary Science Letters, v. 222, p. 43–60.

Brasier, M.D., Green, O.R., Jephcoat, A.P., Kleepe, A.K., Van Kranendonk, M.J., Lindsay, F., Steele, A., and Grassineau, N.V., 2002, Questioning the evidence for Earth's oldest fossils: Nature, v. 416, p. 76–81.

Buick, R., and Barnes, K.R., 1984, Cherts in the Warrawoona Group: Early Archaean silicified sediments deposited in shallow-water environments, *in* Muhling, J.R., Groves, D.I., and Blake, T.S., eds., Archean and Proterozoic basins of the Pilbara, Western Australia: Geology Department (Key Centre) and University Extension, The University of Western Australia Publication 9, p. 37–53.

Byerly, G.R., Kröner, A., Lowe, D.R., Todt, W., and Walsh, M.M., 1986, Stromatolites from the 3,300–3,500 Myr Swaziland Supergroup, Barberton Mountain Land, South Africa: Nature, v. 319, p. 489–491, doi: 10.1038/319489a0.

Cady, S.L., and Farmer, J.D., 1996, Fossilization processes in siliceous thermal springs: Trends in preservation along thermal gradients, *in* Brock, G.R., and Goode, J.A., eds., Evolution of Hydrothermal Systems on Earth (and Mars?): New York, Wiley, p. 150–170.

Condie, K.C., 1991, Another look at rare-earth elements in shales: Geochimica et Cosmochimica Acta, v. 55, p. 2527–2531, doi: 10.1016/0016-7037(91)90370-K.

Condie, K.C., 1997, Sources of Proterozoic mafic dyke swarms: Constraints from Th/Ta and La/Yb ratios: Precambrian Research, v. 81, p. 3–14, doi: 10.1016/S0301-9268(96)00020-4.

Conway Morris, S., 1989, The Burgess shale faunas and the Cambrian explosion: Science, v. 246, p. 339–346.

de Ronde, C.E.J., Channer, D.M., Faure, K., Bray, C.J., and Spooner, T.C., 1997, Fluid chemistry of Archean seafloor hydrothermal vents: Implications for the composition of circa 3.2 Ga seawater: Geochimica et Cosmochimica Acta, v. 61, p. 4025–4042.

de Vries, S.T., 2004, Early Archaean sedimentary basins: Depositional environment and hydrothermal systems: Geologica Utraiectina, v. 244, 160 p.

de Wit, M., Hart, R., Martin, A., and Abbott, P., 1982, Archean abiogenic and probable biogenic structures associated with mineralized hydrothermal vent systems and regional metasomatism, with implications for greenstone belt studies: Economic Geology and the Bulletin of the Society of Economic Geologists, v. 77, p. 1783–1802.

Douville, E., Bienvenu, P., Charlou, J.L., Donval, J.P., Fouquet, Y., Appriou, P., and Gamo, T., 1999, Yttrium and rare earth elements in fluids from various deep-sea hydrothermal systems: Geochimica et Cosmochimica Acta, v. 63, p. 627–643, doi: 10.1016/S0016-7037(99)00024-1.

Duchac, K.C., 1986, Metasomatic alteration of a komatiic sequence into chert [M.S. thesis]: Baton Rouge, Louisiana State University, 240 p.

Dunlop, J.S.R., 1978, Shallow-water sedimentation at North Pole, Pilbara Block, Western Australia: Geology, Department and University Extension Publication, v. 2, p. 390–438.

Dunlop, J.S.R., and Buick, R., 1981, Archaean epiclastic sediments derived from mafic volcanics, North Pole, Pilbara, Western Australia: Geological Society of Australia Special Publications, v. 7, p. 225–233.

Eugster, H.P., 1967, Hydrous sodium silicates from Lake Magadi, Kenya: Precursors of bedded cherts: Science, v. 157, p. 1177–1180.

Evensen, N.M., Hamilton, P.J., and O'Nions, R.K., 1978, Rare earth abundances in chondritic meteorites: Geochimica et Cosmochimica Acta, v. 42, p. 1199–1212, doi: 10.1016/0016-7037(78)90114-X.

Farmer, J.D., and Des Marais, D.J., 1999, Exploring for a record of ancient Martian life: Journal of Geophysical Research, v. 104, p. 26,977–26,995.

Fedo, C.M., and Whitehouse, M.J., 2002, Metasomatic origin of quartz-pyroxene rock, Akilia, Greenland, and implications for Earth's earliest life: Science, v. 296, p. 1448–1452, doi: 10.1126/science.1070336.

Föllmi, K.B., 1990, Condensation and phosphogenesis: Example of the Helvetic mid-Cretaceous (northern Tethyan margin), *in* Notholt, A.J.G, and Jarvis, I., eds., Phosphorite Research and Development: Geological Society [London] Special Publication 52, p. 237–252.

Fournier, R.O., and Rowe, J.J., 1966, Estimation of underground temperatures from the silica content of water from hot-springs and wet-steam wells: American Journal of Science, v. 264, p. 685–697.

Gallien, J.P., Orberger, B., Pinti, D.L., Wagner, C., Fialin, M., Daudin, L., and Hashizume, K., 2003, Mineralogy and geochemistry of an Archaean chert: In quest of N-sites: Geochimica et Cosmochimica Acta, v. 67, p. A115.

Grenne, T., and Slack, J.F., 2003a, Bedded jaspers of the Ordovician Lokken ophiolite, Norway: Seafloor deposition and diagenetic maturation of hydrothermal plume-derived silica-iron gels: Mineralium Deposita, v. 38, p. 625–639, doi: 10.1007/s00126-003-0346-3.

Grenne, T., and Slack, J.F., 2003b, Paleozoic and Mesozoic silica-rich seawater: Evidence from hematitic chert (jasper) deposits: Geology, v. 31, p. 319–322, doi: 10.1130/0091-7613(2003)031<0319:PAMSRS>2.0.CO;2.

Gross, G.A., 1980, A classification of iron formations based on depositional environments: Canadian Mineralogist, v. 18, p. 171–187.

Grotzinger, J.P., and Knoll, A.H., 1995, Anomalous carbonate precipitates in the Precambrian the key to the Permian?: Palaios, v. 10, p. 578–596.

Halbach, M., Halbach, P., and Lueders, V., 2002, Sulfide-impregnated and pure silica precipitates of hydrothermal origin from the central Indian Ocean: Chemical Geology, v. 182, p. 357–375, doi: 10.1016/S0009-2541(01)00323-0.

Hanor, J.S., and Duchac, K., 1990, Isovolumetric silicification of early Archaean komatiites: Geochemical mass balances and constraints on origin: The Journal of Geology, v. 98, p. 863–877.

Herzig, P.M., Becker, K.P., Stoffers, P., Bäcker, H., and Blum, N., 1988, Hydrothermal silica chimney fields in the Galapagos spreading center at 86°W: Earth and Planetary Science Letters, v. 89, p. 261–272, doi: 10.1016/0012-821X(88)90115-X.

Hofmann, A., 2004, Sedimentary versus hydrothermal processes for the origin of carbonaceous cherts in the Barberton Greenstone belt, *in* Reimold, W.U., and Hofmann, A., eds., Field Forum: Processes on the Early Earth, Kaapvaal Craton, South Africa: Johannesburg, Abstracts, p. 35–37.

Holland, H.D., 1973, The oceans: A possible source of iron in iron-formations: Economic Geology and the Bulletin of the Society of Economic Geologists, v. 68, p. 1169–1172.

Horan, M.F., Morgan, J.W., Grauch, R.I., Coveney, J.R.M., Murowchick, J.B., and Hulbert, L.J., 1994, Rhenium and osmium isotopes in black shales and Ni-Mo-PGE-rich sulfide layers, Yukon Territory, Canada, and

Hunan and Guizhou provinces, China: Geochimica et Cosmochimica Acta, v. 58, p. 257–265.

Huston, D.L., Sie, S.H., and Suter, G.F., 1995, Selenium and its importance to the study of ore genesis: The theoretical basis and its application to volcanic-hosted massive sulfide deposits using pixeprobe analysis: Nuclear Instruments & Methods in Physics Research, Section B, Beam Interactions with Materials and Atoms, v. 104, p. 476–480, doi: 10.1016/0168-583X(95)00462-9.

Isozaki, Y., Kabashima, T., Ueno, Y., Kitajima, K., Maruyama, S., Kato, Y., and Terabayashi, M., 1999, Early Archean mid-ocean ridge rocks and early life in the Pilbara Craton, W. Australia, [abs.]: Eos (Transactions, American Geophysical Union), v. 78, Supplement, p. 399.

Juniper, S.K., and Fouquet, Y., 1988, Filamentous iron-silica deposits from modern and ancient hydrothermal sites: Canadian Mineralogist, v. 26, p. 859–869.

Kato, Y., and Nakamura, K., 2003, Origin and global tectonic significance of early Archean cherts from the Marble Bar greenstone belt, Pilbara Craton, Western Australia: Precambrian Research, v. 125, p. 191–243, doi: 10.1016/S0301-9268(03)00043-3.

Kimberley, M.M., 1989, Exhalative origins of iron formations: Ore Geology Reviews, v. 5, p. 130–145, doi: 10.1016/0169-1368(89)90003-6.

Kitajima, K., Maruyama, S., Utsunomiya, S., and Liou, J.G., 2001, Seafloor hydrothermal alteration at an Archaean mid-ocean ridge: Journal of Metamorphic Geology, v. 19, p. 583–597, doi: 10.1046/j.0263-4929.2001.00330.x.

Knauth, L.P., and Lowe, D.R., 1978, Oxygen isotope geochemistry of cherts from the Onverwacht Group (3.4 billion years), Transvaal, South Africa, with implications for secular variations in the isotopic composition of cherts: Earth and Planetary Science Letters, v. 41, p. 209–222, doi: 10.1016/0012-821X(78)90011-0.

Lepland, A., Van Zuilen, M., and Arrhenius, G., 2002, Origin and biologic significance of graphite and apatite in early Archean supracrustal rocks from Isua belt and Akilia association: Geochimica et Cosmochimica Acta, v. 66, p. A448.

Lindsay, J.F., McKay, D.S., and Allen, C.C., 2003, Earth's earliest biosphere—A proposal to develop a collection of curated Archean geologic reference materials: Astrobiology, v. 3, p. 739–754, doi: 10.1089/153110703322736060.

Lowe, D.R., 1999, Petrology and sedimentology of cherts and related silicified sedimentary rocks in the Swaziland Supergroup, *in* Lowe, D.R., and Byerly, G.R., eds., Geologic evolution of the Barberton Greenstone Belt, South Africa: Geological Society of America Special Paper 329, p. 83–114.

Lowe, D.R., and Byerly, G.R., 1999, Geologic evolution of the Barberton Greenstone Belt, South Africa: Geological Society of America Special Paper 329, 324 p.

Lowe, D.R., and Worrell, G.F., 1999, Sedimentology, mineralogy, and implications of silicified evaporites in the Kromberg Formation, Barberton Greenstone Belt, South Africa, *in* Lowe, D.R., and Byerly, G.R., eds., Geologic evolution of the Barberton Greenstone Belt, South Africa: Geological Society of America Special Paper 329, p. 167–187.

Lydon, J.W., 1984, Volcanogenic massive sulphide deposits, I, A descriptive model, *in* Roberts, R.G., and Shean, P.A., eds., Ore Deposit Models, Geoscience Canada Reprint Series, Volume 3, p. 145–153.

Mao, J., Lehmann, B., Du, A., Zhang, G., Ma, D., Wand, Y., Zeng, M., and Kerrich, R., 2002, Re-Os dating of polymetallic Ni-Mo-PGE-Au mineralization in Lower Cambrian black shales and its geologic signification: Economic Geology and the Bulletin of the Society of Economic Geologists, v. 47, p. 1051–1061.

Mills, R.A., and Elderfield, H., 1995, Rare earth element geochemistry of hydrothermal deposits from the active TAG Mound, 26°N Mid-Atlantic Ridge: Geochimica et Cosmochimica Acta, v. 59, p. 3511–3524, doi: 10.1016/0016-7037(95)00224-N.

Mojzsis, S.L., Arrhenius, G., and Friend, C.R.L., 1996, Evidence for life on Earth before 3,800 million years ago: Nature, v. 384, p. 55–57, doi: 10.1038/384055a0.

Muzuka, A.N.N., Macko, S.A., and Pedersen, T.F., 1991, Stable carbon and nitrogen isotope compositions of organic matter from Site 724 and Site 725, Oman margin, *in* Prell, W.L., and Niitsuma, N., eds., Initial Report ODP Leg 117: Proceedings of the Ocean Drilling Program, Scientific Results, v. 117, p. 571–586.

Myers, J.S., 2001, Protoliths of the 3.8–3.7 Ga Isua greenstone belt: West Greenland: Precambrian Research, v. 105, p. 129–141, doi: 10.1016/S0301-9268(00)00108-X.

Nealson, K.H., and Myers, C.R., 1990, Iron reduction by bacteria: A potential role in the genesis of banded iron formations: American Journal of Science, v. 290, p. 35–45.

Nedachi, M., 2004, New discoveries from the Archean Biosphere Drilling Project (ABDP) [abs.]: Eos (Transactions, American Geophysical Union), v. 85, Supplement, B32B-03.

Nijman, W., de Bruijne, K.C.H., and Valkering, M.E., 1998, Growth fault control of early Archaean cherts, barite mounds and chert-barite veins, North Pole Dome, Eastern Pilbara, Western Australia: Precambrian Research, v. 88, p. 25–52, doi: 10.1016/S0301-9268(97)00062-4.

Orberger, B., and Alleweldt, J., 1994, Contribution to the petrogenesis of the platinum palladium-bearing black dunites of the Acoje block, Zambales ophiolite, Philippines; selenium and sulfur-contents, clinopyroxenes, initial weathering: Journal of Southeast Asian Earth Sciences, v. 9, p. 229–239, doi: 10.1016/0743-9547(94)90030-2.

Orberger, B., Pasava, J., Gallien, J.-P., Daudin, L., and Trocellier, P., 2003, Se, As, Mo, Ag, Cd, In, Sb, Pt, Au, Tl, Re traces in biogenic and abiogenic sulfides from black shales (Selwyn Basin, Yukon territories, Canada): A nuclear microprobe study: Nuclear Instruments & Methods in Physics Research, Section B, Beam Interactions with Materials and Atoms, v. 210, p. 441–448, doi: 10.1016/S0168-583X(03)01073-5.

Orberger, B., Gallien, J.P., Pinti, D.L., Fialin, M., Daudin, L., Gröcke, D.R., and Pasava, J., 2005a, Nitrogen and carbon partitioning in diagenetic and hydrothermal minerals from Paleozoic black shales (Selwyn Basin, Yukon Territories, Canada): Chemical Geology, v. 218, p. 249–264.

Orberger, B., Wagner, C., Vymalanova, A., Pasava, J., Kribek, B., and Gallien, J.P., 2005b, Rare metal sequestration and mobility in mineralized black shales from the Zunyi region, South China, *in* Mao, J., Bierlein, F.P., eds., Mineral Deposit Research, meeting the global challenge: Springer Verlag, v. 1, p. 167–171.

Paris, I., Stanistreet, I.G., and Hughes, M.J., 1985, Cherts of the Barberton Greenstone Belt interpreted as products of submarine exhalative activity: The Journal of Geology, v. 93, p. 111–130.

Pinti, D.L., and Hashizume, K., 2001, N-15-depleted nitrogen in early Archean kerogens: Clues on ancient marine chemosynthetic-based ecosystems? A comment to Beaumont, V., and Robert, F., 1999, Precambrian Research v. 96, p. 62–82: Precambrian Research, v. 105, p. 85–88, doi: 10.1016/S0301-9268(00)00100-5.

Pinti, D.L., Matsuda, J., and Maruyama, S., 2001a, Anomalous xenon in Archean cherts from Pilbara Craton, Western Australia: Chemical Geology, v. 175, p. 387–395, doi: 10.1016/S0009-2541(00)00331-4.

Pinti, D.L., Hashizume, K., and Matsuda, J., 2001b, Nitrogen and argon signatures in 3.8 to 2.8 Ga metasediments: Clues on the chemical state of the Archean ocean and the deep biosphere: Geochimica et Cosmochimica Acta, v. 65, p. 2301–2315, doi: 10.1016/S0016-7037(01)00590-7.

Pinti, D.L., Hashizume, K., Philippot, P., Foriel, J., and Rey, P., 2003, Nitrogen quest in Archean metasediments of Pilbara, Australia: Geochimica et Cosmochimica Acta, v. 67, p. A379.

Pirajno, F., and Grey, K., 2002, Chert in the Palaeoproterozoic Bartle Member, Killara Formation, Yerrida Basin, Western Australia: A rift-related playa lake and thermal spring environment?: Precambrian Research, v. 113, p. 169–192, doi: 10.1016/S0301-9268(01)00196-6.

Préat, A., Mamet, B., de Jong, J., Durlet, C., Morano, S., and Matielli, N., 2004, Origine de la pigmentation de l'Ammonitico Rosso d'Italie du nord (Jurassique moyen, region de Verone): Biosédimentologie; diagenèse et géochimie isotopique, *in* Camoin, G., and Gautret, P., eds., Microbialite

and microbial communities in sedimentary systems: Paris, Workshop, 6–9 September, Publications de l'Association Sédimentologique Français, v. 46, p. 79–82.

Rau, G.H., Arthur, M.A., and Dean, W.E., 1987, 15N/14N variations in Cretaceous Atlantic sedimentary sequences: Implication for past changes in marine nitrogen biogeochemistry: Earth and Planetary Science Letters, v. 82, p. 269–279, doi: 10.1016/0012-821X(87)90201-9.

Renaut, R.W., Jones, B., Tiercelin, J.J., and Tarits, C., 2002, Sublacustrine precipitation of hydrothermal silica in rift lakes: Evidence from Lake Baringo, central Kenya Rift Valley: Sedimentary Geology, v. 148, p. 235–257, doi: 10.1016/S0037-0738(01)00220-2.

Rouchon, V., Pinti, D.L., Gallien, J.P., Orberger, B., Daudin, L., and Westall, F., 2005, NRA analyses of N and C in hydromuscovite from a 3.5 Ga chert from Kitty's Gap, Pilbara, Australia: Nuclear Instruments and Methods in Physics Research, v. B231, p. 536–540.

Schidlowski, M., Hayes, J.M., and Kaplan, I.R., 1983, Isotopic inferences of ancient biochemistries: Carbon, sulfur, hydrogen, and nitrogen, *in* Schopf, W.J., ed., Earth's Earliest Biosphere: Princeton, Princeton University Press, p. 149–186.

Schubel, K.A., and Simonson, B.M., 1990, Petrography and diagenesis of cherts from Lake Magadi, Kenya: Journal of Sedimentary Petrology, v. 60, p. 761–776.

Siever, R., 1992, The silica cycle in the Precambrian: Geochimica et Cosmochimica Acta, v. 56, p. 3265–3272, doi: 10.1016/0016-7037(92)90303-Z.

Steiner, M., Wallis, E., Erdtmann, B.D., Yuanlong, Z., and Yang, R., 2001, Submarine-hydrothermal exhalative ore layers in black shales from South China and associated fossils—Insights into a Lower Cambrian facies and bio-evolution: Paleogeography, Paleoclimatology, Paleoecology, v. 169, p. 165–191, doi: 10.1016/S0031-0182(01)00208-5.

Sugitani, K., 1992, Geochemical characteristics of Archean cherts and other sedimentary rocks in the Pilbara Block, Western Australia: Evidence for Archean seawater enriched in hydrothermally derived iron and silica: Precambrian Research, v. 57, p. 21–47, doi: 10.1016/0301-9268(92)90093-4.

Sugitani, K., Yamamoto, K., Wada, H., Binu-Lal, S.S., and Yoneshige, M., 2002, Geochemistry of Archean carbonaceous cherts deposited at immature island-arc setting in the Pilbara Block, Western Australia: Sedimentary Geology, v. 151, p. 45–66, doi: 10.1016/S0037-0738(01)00230-5.

Sweeney, R.E., Liu, K.K., and Kaplan, I.R., 1978, Oceanic nitrogen isotopes and their uses in determining the source of sedimentary nitrogen: Department of Scientific Industrial Resources New Zealand Bulletin, v. 220, p. 9–26.

Takano, Y., Kobayashi, K., Yamanaka, T., Marumo, K., and Urabe, T., 2004, Amino acids in the 308[deg]C deep-sea hydrothermal system of the Suiyo Seamount, Izu-Bonin Arc, Pacific Ocean: Earth and Planetary Science Letters, v. 219, p. 147–153, doi: 10.1016/S0012-821X(03)00699-X.

Tarasov, V.G., Gebruk, A.V., Shulkin, V.M., Kamenev, V.M., Fadeev, V.I., Kosmynin, V.N., Malakhov, V.V., Starynin, D.A., and Obzhirov, A.I., 1999, Effect of shallow-water hydrothermal venting on the biota of Matupi Harbour (Rabaul Caldera, New Britain Island, Papua New Guinea): Continental Shelf Research, v. 19, p. 79–116, doi: 10.1016/S0278-4343(98)00073-9.

Tebo, B.M., Ghiorse, W.C., van Waasbergen, L.G., Siering, P.L., and Caspi, R., 1997, Bacterially mediated mineral formation: Insights into manganese (II)-oxidation from molecular genetic and biochemical studies, *in* Banfield, J.F., and Nealson, K.H., eds., Geomicrobiology: Interactions between microbes and minerals, Reviews in Mineralogy, Volume 35: Washington, D.C., Mineralogical Society of America, p. 225–260.

Thorpe, R.I., Hickman, A.H., Davis, D.W., Mortensen, J.K., and Trendall, A.F., 1992, U-Pb zircon geochronology of Archean felsic units in the Marble Bar Region, Pilbara Craton, Western Australia: Precambrian Research, v. 56, p. 169–189, doi: 10.1016/0301-9268(92)90100-3.

Ueno, Y., Yoshioka, H., Maruyama, S., and Isozaki, Y., 2004, Carbon isotopes and petrography of kerogens in similar to 3.5-Ga hydrothermal silica dikes in the North Pole area, Western Australia: Geochimica et Cosmochimica Acta, v. 68, p. 573–589, doi: 10.1016/S0016-7037(03)00462-9.

Umeda, M., 2003, Precipitation of silica and formation of chert-mudstone-peat association in Miocene coastal environments at the opening of the Sea of Japan: Sedimentary Geology, v. 161, p. 249–268, doi: 10.1016/S0037-0738(03)00117-9.

Uyeda, S., 1987, Active hydrothermal mounds in the Okinawa back arc trough [abs.]: Eos (Transactions, American Geophysical Union), v. 68, p. 737.

Van Kranendonk, M.J., Hickman, A.H., Williams, I.R., and Nijman, W., 2001, Archaean geology of the East Pilbara granite-greenstone terrane, Western Australia—A field guide: Perth, Western Australia, Geological Survey of Western Australia, 134 p.

van Zuilen, M.A., Lepland, A., Terranes, J., Finarelli, J., Wahlen, M., and Arrhenius, G., 2003, Graphite and carbonates in the 3.8 Ga old Isua Supracrustal Belt, southern West Greenland: Precambrian Research, v. 126, p. 331–348.

Walsh, M., 1992, Microfossils and possible microfossils from the early Archean Onverwacht group, Barberton Mountain Land, South Africa: Precambrian Research, v. 54, p. 271–293, doi: 10.1016/0301-9268(92)90074-X.

Walsh, M.M., and Lowe, D.R., 1999, Modes of accumulation of carbonaceous matter in the early Archean: A petrographic and geochemical study of the carbonaceous cherts of the Swaziland Supergroup, *in* Lowe, D.R., and Byerly, G.R., eds., Geologic evolution of the Barberton Greenstone Belt, South Africa:: Geological Society of America Special Paper 329, p. 115–132.

Westall, F., 2005, The geological context for the origin of life and the mineral signatures of fossil life, *in* Gardaud, M., Barbier, B., Martin, H., and Reisse, G., eds., Lectures in Astrobiology, Vol. I: Berlin, Springer-Verlag (in press).

Westall, F., de Wit, M.J., Dann, J., van der Gaast, S., de Ronde, C.E.J., and Gerneke, D., 2001, Early Archean fossil bacteria and biofilms in hydrothermally influenced sediments from the Barberton greenstone belt, South Africa: Precambrian Research, v. 106, p. 93–116, doi: 10.1016/S0301-9268(00)00127-3.

Westall, F., Orberger, B., Rouchon, V., Rouzaud, J.N., and Wright, I., 2004, On the identification of early Archaean microfossils in cherts from Barberton and the Pilbara, *in* Reimold, W.U., and Hofmann, A., compilers, Field Forum: Processes on the early Earth, Kaapvaal Craton, South Africa: Abstracts: Johannesburg, p. 94–97.

Westall, F., de Vries, S.T., Nijman, W., Rouchon, V., Orberger, B., Pearson, V., Watson, J., Verchovsky, A., Wright, I., Rouzaud, J.-N., Marchesini, D., and Severine, A., 2006, this volume, The 3.466 Ga Kitty's Gap Chert, an early Archean microbial ecosystem, *in* Reimold, W.U., and Gibson, R.L., Processes on the early Earth: Geological Society of America Special Paper 405, doi: 10.1130/2006.2405(07).

Williams, L.A., and Crerar, D.A., 1985, Silica diagenesis, II, General mechanism: Journal of Sedimentary Petrology, v. 55, p. 312–321.

Wirth, R., 2004, Focused Ion Beam (FIB): A novel technology for advanced application of micro- and nanoanalysis in geosciences and applied mineralogy: European Journal of Mineralogy, v. 16, p. 863–876, doi: 10.1127/0935-1221/2004/0016-0863.

Manuscript Accepted by the Society 4 October 2005

Geological Society of America Special Papers

Microfacies and origin of some Archean cherts (Pilbara, Australia)

Beate Orberger, Virgile Rouchon, Frances Westall, et al.

Geological Society of America Special Papers 2006;405; 133-156
doi:10.1130/2006.2405(08)